2017-01-01

Investigation Of Earthquake And Geyser Activity From Short-Term Nodal Array Deployment Centered At Old Faithful Geyser

Susana I. Garcia
University of Texas at El Paso, susana.i.garcia13@gmail.com

INVESTIGATION OF EARTHQUAKE AND GEYSER ACTIVITY FROM SHORT-TERM NODAL ARRAY DEPLOYMENT CENTERED AT OLD FAITHFUL GEYSER

SUSANA IVONNE GARCIA

Master's Program in Geophysics

APPROVED:

Marianne Karplus, Ph.D., Chair

Aaron Velasco, Ph.D.

Wen-Whai Li, Ph.D., P.E.

Charles Ambler, Ph.D.
Dean of the Graduate School

Dedication

For David

INVESTIGATION OF EARTHQUAKE AND GEYSER ACTIVITY FROM SHORT-TERM NODAL ARRAY DEPLOYMENT CENTERED AT OLD FAITHFUL GEYSER

by

SUSANA IVONNE GARCIA, B.S.

THESIS

Presented to the Faculty of the Graduate School of

The University of Texas at El Paso

in Partial Fulfillment

of the Requirements

for the Degree of

MASTER OF SCIENCE

Department of Geological Sciences

THE UNIVERSITY OF TEXAS AT EL PASO

December 2017

Acknowledgements

First and foremost, I would like to thank the amazing geophysics professors at UTEP for providing a quality education and learning experience with professors that are genuinely concerned with your success, this includes Dr. Marianne Karplus, Dr. Aaron Velasco and Dr. Diane Doser. And a thank you to Dr. Wen-Whai Li in the Engineering department who afforded me the opportunity to participate in an Air Quality internship. I am also very grateful for the many classmates that I met while at UTEP who were often kind, knowledgeable and offered their assistance to work together for various coursework and research. My gratitude also goes out to my family who helped me during the process of obtaining my Master's.

Abstract

Yellowstone National Park is home to an active caldera, centrally located on the North American continent. Several studies have concluded the existence of a hotspot that fuels the hydrothermal, geothermal and earthquake activity in the Yellowstone region. The geologic record of Yellowstone contains multiple layers of volcanic deposits that indicate the region experienced three previous massive volcanic eruptions dating back 2.05Mya, 1.2Mya and the most recent 640,000 years ago. Yellowstone is also home to one of the largest geothermal areas in the world. With this study, an in-depth look at seismicity and geyser events recorded within an active geothermal region, specifically, the Upper Geyser Basin that includes the Old Faithful Geyser (OFG) will provide a new perspective of the immediate subsurface. A temporary deployment of a three-dimensional array of 133 Z-Land Nodal geophones recorded passive data in the OFG area from November 2-14, 2015. The deployment occurred as a joint venture with the University of Utah, in which they focused their study on processing ambient noise and seismic recordings of the hydrothermal activity with the same dataset. Our analysis of the data will focus on the regional and teleseismic earthquakes as well as some of the geyser eruption events as picked up by the array. The constant activity of Yellowstone region provides frequent seismic sources, which could provide useful information for seismic interpretation of the complex subsurface.

One of the objectives of this study included signal processing of local micro-seismic events and teleseismic events. Spectral images, Fast Fourier Transform (FFT), phase and amplitude, analysis are examined for a variety of recorded seismic and geyser events. We also created ground motion visualizations from seismic and geyser events. These visualizations show the propagation of waves within the Upper Geyser Basin as they travel through the array.

Table of Contents

List of Tables

List of Figures

Introduction

The Yellowstone National Park houses several calderas which formed from previous explosive volcanic eruptions dating 2.05 Ma to 0.64Ma. Remains of these calderas trend southwest (oldest) to northeast (youngest) across the Yellowstone Snake River Plain (YSRP). Each caldera remnant represents evidence of the North American plate southwestward movement relative to the mantle plume (Fig. 1). (Christiansen, 1972) Mantle plumes originate deep within the Earth and often lead to the formation of volcanic features on the surface. Due to the large volume of magma beneath it and its capability for super-eruptions, Yellowstone has been labeled a "supervolcano" and is one of the largest active geothermal areas on Earth. The most recently known volcanic eruption at Yellowstone occurred 640,000 years ago that deposited tuff formations found in the region. This ancient caldera contains a zone of active seismicity from faulting, resurgent domes, and hydrothermal features such as geysers and hot springs. (Pierce and Morgan, 1992) Two resurgent domes located within the boundaries of the caldera are Sour Creek (SC) and Mallard Lake (ML), in which, Old Faithful Geyser (OFG) can be found just northeast of ML dome.

OFG in the Upper Geyser Basin at Yellowstone, produces large hydrothermal explosions approximately every 60-110 minutes (NPS, 2017). OFG spouts out steam and water to heights up to 130 feet with the highest known recording at 190 feet, and previous observations of eruptions lasting up to five minutes. (USGS, 2016) Water expelled by the geyser has been measured at 95.6ºC with up to 177ºC temperature in the case of steam emissions. Old Faithful often ejects between ~3700 gallons to 8400 gallons of water depending on the duration of the eruption. (NPS, 2016) The hydrothermal water measures neutral to alkaline in pH and rich in dissolved chloride and silica (SiO_2) which once cooled at the surface forms silica sinter that can be seen draped around the geyser opening. (Hurwitz, 2016) The consistency of geyser eruptions at Yellowstone are sustained by the continual recharge from numerous lakes, rivers and aquifers in the region based on the findings that support most of the water sources supplying the geyser

come from rain and snow (Old Faithful Science Review board, 2014). The Upper Geyser Basin contains a wide variety of geysers with spasmodic eruption times and other hydrothermal behaviors.

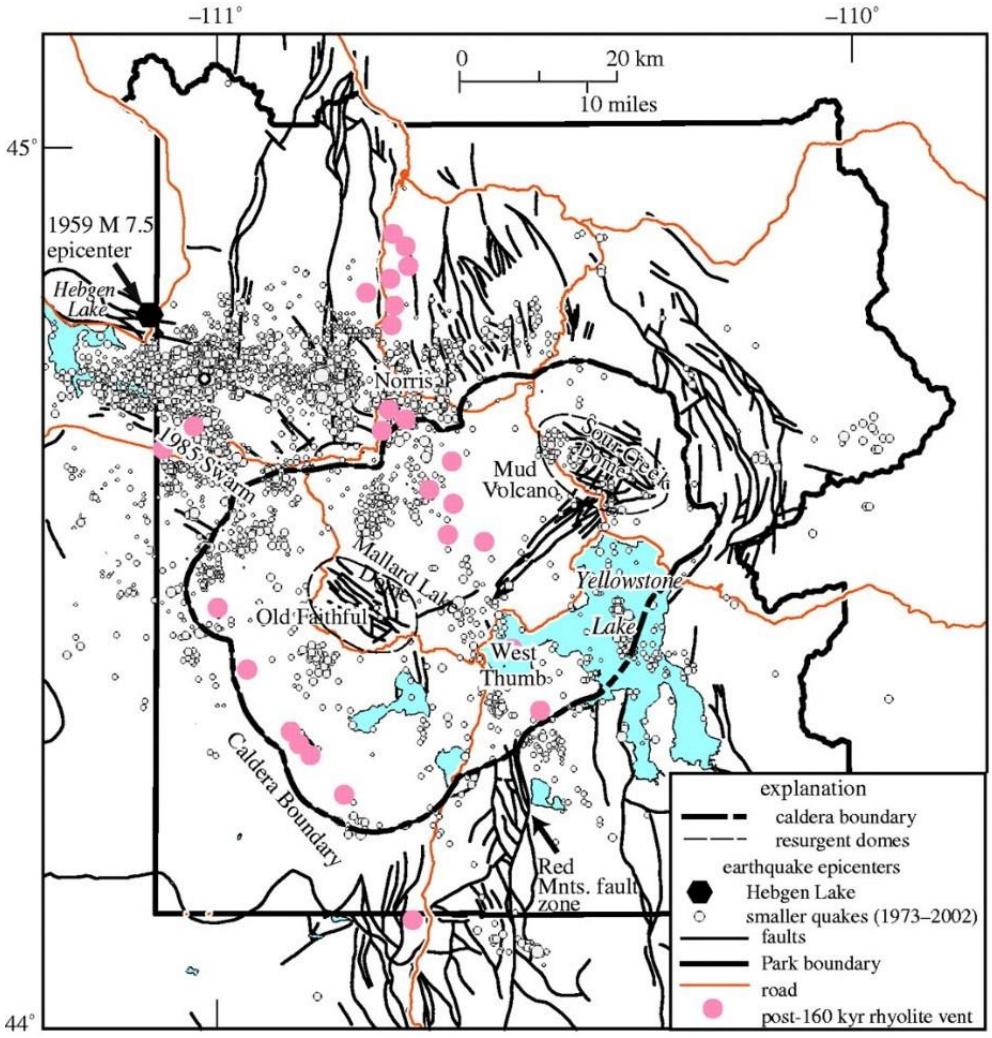

Figure A: Overview of Map of Yellowstone National Park

Map taken from Lowenstern (2006) details the region immediately surrounding the Yellowstone National Park. Depicted are the two resurgent domes Mallard Lake (ML) and Sour Creek (SC) within the caldera boundary. Faults and previous earthquake events are also included in this figure and the notable large magnitude 7.5 earthquake on Hebgen Lake that occurred in 1959.

This experiment recorded seismic activity caused by both hydrothermal and earthquake events. Using the data to create subsurface "mapping" of the geyser plumbing and deeper crustal structures became the initial drive for this study. Colleagues at the University of Utah focused

primarily on characterizing signals generated by the hydrothermal features such as bubble collapse. A previous study with similar array distribution at OFG concentrated on the analysis of tremors caused by cavitation, which uncovered the existence of a lateral cavity that plays a large role in OFG dynamics. (Vandemeulebrouck, et. al., 2013) In this project, identifying signals from local and teleseismic earthquakes recorded on this dense array proved useful in identifying changes in seismic wave velocity beneath the array.

Chapter 1: Background Information

Several studies conducted in the Yellowstone region have led many researchers to postulate a bevy of geological processes and responses as part of the dynamical forces that have over time led to the region's current condition, and the path it may take in the future. In this chapter, discussions will focus on the historical geology and seismic events taken from previous studies and observations. Continual research of the region can lead to a better understanding of the subsurface structure and the processes that could one day offer sufficient information towards life-saving predictions.

Geological Background

A few of the geological features seen at Yellowstone such as geysers, fumaroles, pools, hot springs, and mudpots are the most active products that provide evidence of underground thermal features from an active hotspot. Earthquakes and tremors are response to the continued movement of subsurface lithology that continually adjust to the active hydro and thermal energy that synergistically supports the transformation of the landscape and subsurface structures. The infamous hotspot creates a long list of active features that have continued to occur in the region for several million years.

In this section, brief descriptions of Yellowstone's stratigraphy will be noted as they were taken from a previous study. The Yellowstone Quaternary stratigraphy represents three volcanism cycles comprised mostly of basalts and rhyolites which are properly cataloged and described by Christiansen and Blank (1972). The first caldera formation dates 2.05Ma, the second caldera formed 1.2Ma and the last known eruption occurred 640,000 years ago. Since this study consists of a compact large N-array network over the immediate location of OFG, the geological formations over this area will be detailed herein after. As seen in Figure 2, northeast of OFG is the location of the Mallard Lake resurgent dome that is mostly comprised of rhyolite of the Central Plateau Member (Qpm). The geyser lithology consists of Siliceous hot spring deposits

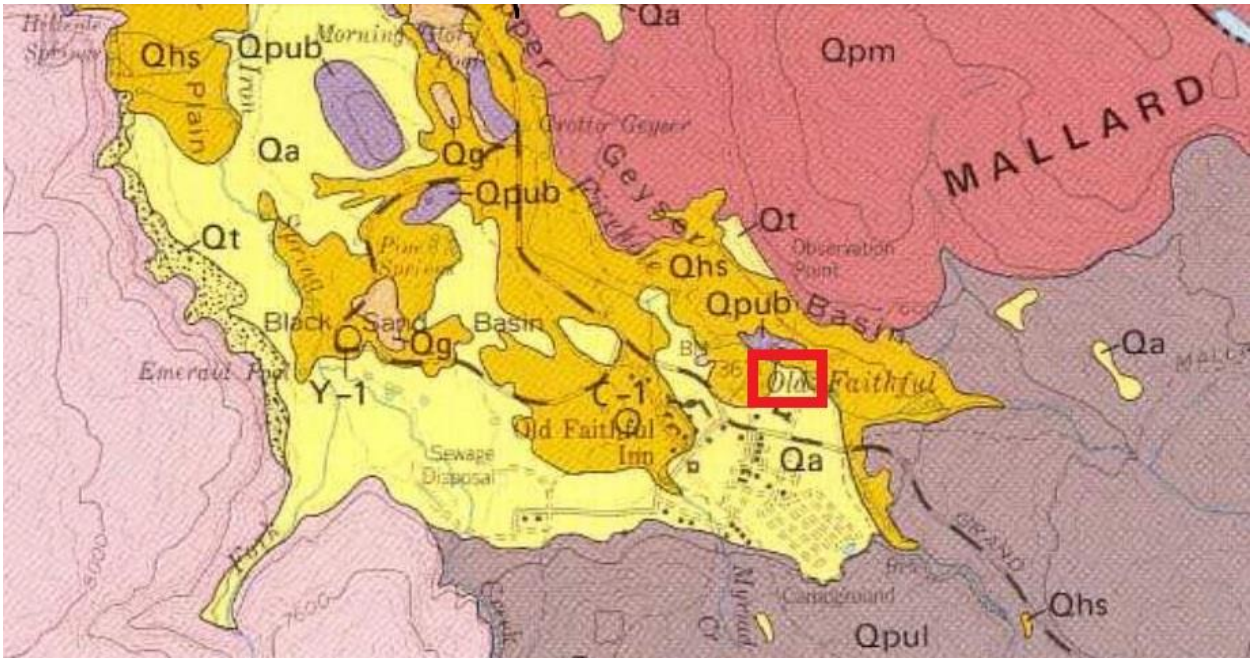

Figure 1.1: Map with detailed rock units surrounding Old Faithful Geyser

The map details specific stratigraphic units around the Old Faithful Geyser. The red square depicts the region in which the experimental deployment of nodes occurred in November 2015. (Christiansen & Black, 1974)

(Qhs) that includes black manganiferous sinter and surrounding this unit is alluvium and glaciofluvial deposits (Qa). The (Qa) unit composition includes unconsolidated sediments from stream-channel, fan deposits, glacial outwash and stream deposits. The (Qhs) is imbedded by lithology of Glacial deposits (Qg) with till lacking morainal form, as well as, a small region of rhyolite from the biscuit basin flow (Qpub) immediately northeast of the geyser and smaller deposits of Tallus and Colluvium (Qt) to the North. Scaup Lake flow (Qpul), also an upper basin member of rhyolite that contains an abundance of phenocrysts of sodic plagioclase and clinopyroxenitic phenocrysts located southeast of the geyser. The quaternary deposits are the evidence of a third eruptive cycle of the rhyolite plateau, 640,000 years ago.

Magma Plume

Yellowstone's dynamic characteristics are the result of a hotspot deep beneath the expanse. This hotspot can be explained by the rise of hot mantle plumes that are solid rock rising

within the Earth's mantle and begin to melt as rock pressure drops on them. (Hyndman, 2009) As a melting of peridotite in the asthenosphere occurs it releases basaltic magma on the surface through volcanos. Pertaining to Yellowstone, as the molten basalt magma rises over a continent it melts surrounding rock to create rhyolite magma that is often the cause of violent eruptions of ash.

DeNosaquo, et. al. (2009) proposed the subsurface plume to be approximately 20km beneath the Moho which is approximately at 40km depth from the surface and expands from the eastern border of the caldera to the southwestern most part of the Snake River Plain. The hotspot reservoir immediately beneath the caldera is fed from the plume by a concentrated quantity of molten sills. The sills that extend the span of the plume and are more dispersed southwest of the Yellowstone caldera, and also supply smaller volcanic activity west of the caldera. In a recent study, scientists suggest that the primary thermal body serving the Yellowstone Region is a magma reservoir detached from the plume itself, as illustrated below. (Figure 1.2)

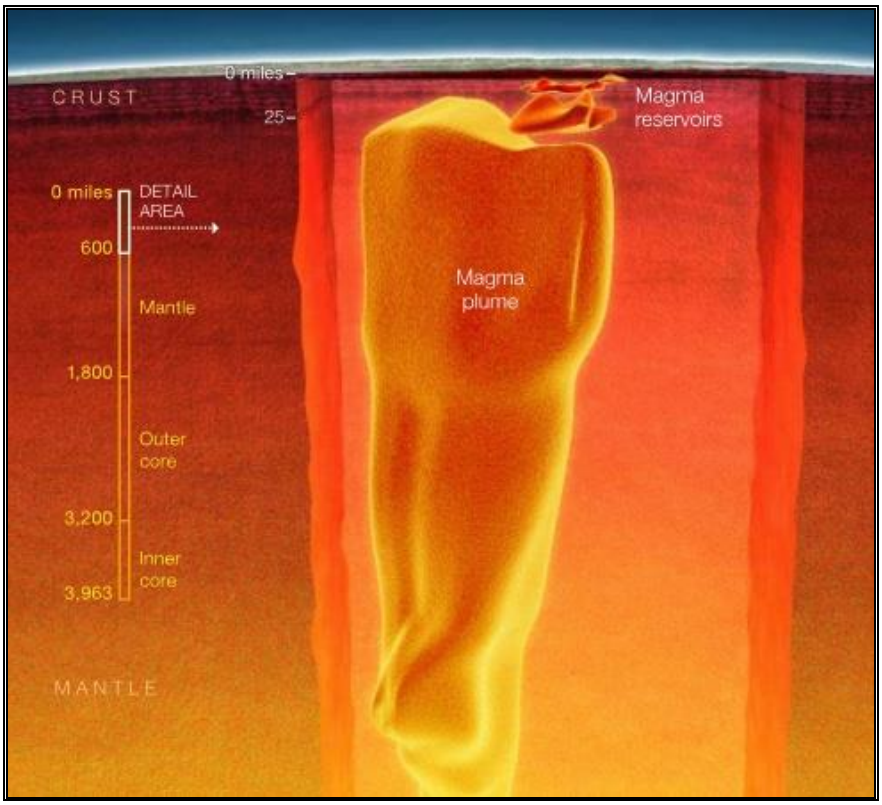

Figure 1.2: Illustration of Magma Plume and reservoirs

Illustration from 'Inside Yellowstone's Supervolcano' short animation from National Geographic. The small reservoir at the top is the primary heat source for the Yellowstone active hydrothermal features.

Volcanic Activity

One of the notable factors regarding the Yellowstone region happens to be the presence of a Supervolcano at its core. The Yellowstone volcano labeled a Supervolcano due to evidence of previous supereruptions. These supereruptions measure an 8 on the Volcanic Explosivity Index (VEI)[1] that is logarithmically scaled, therefore making a VEI=8 100 times larger than an eruption measuring at VEI=6. For reference, the Mt. St. Helens eruption of 1980 measured a 5 on the VEI scale, and the more recent 1991 eruption of Mt. Pinatubo measured as a VEI=6. One important criterion for classifying a supereruption is the volume of ejected pumice and ash greater than 1,000 km^3. Dr. Jake Lowenstern, scientist in charge at the USGS Yellowstone Volcano Observartory, notes an eruption of such magnitude would be enough debris to cover the state of Texas in five feet of ash.

[1] Detailed VEI scale found at the end of this document in the Appendix.

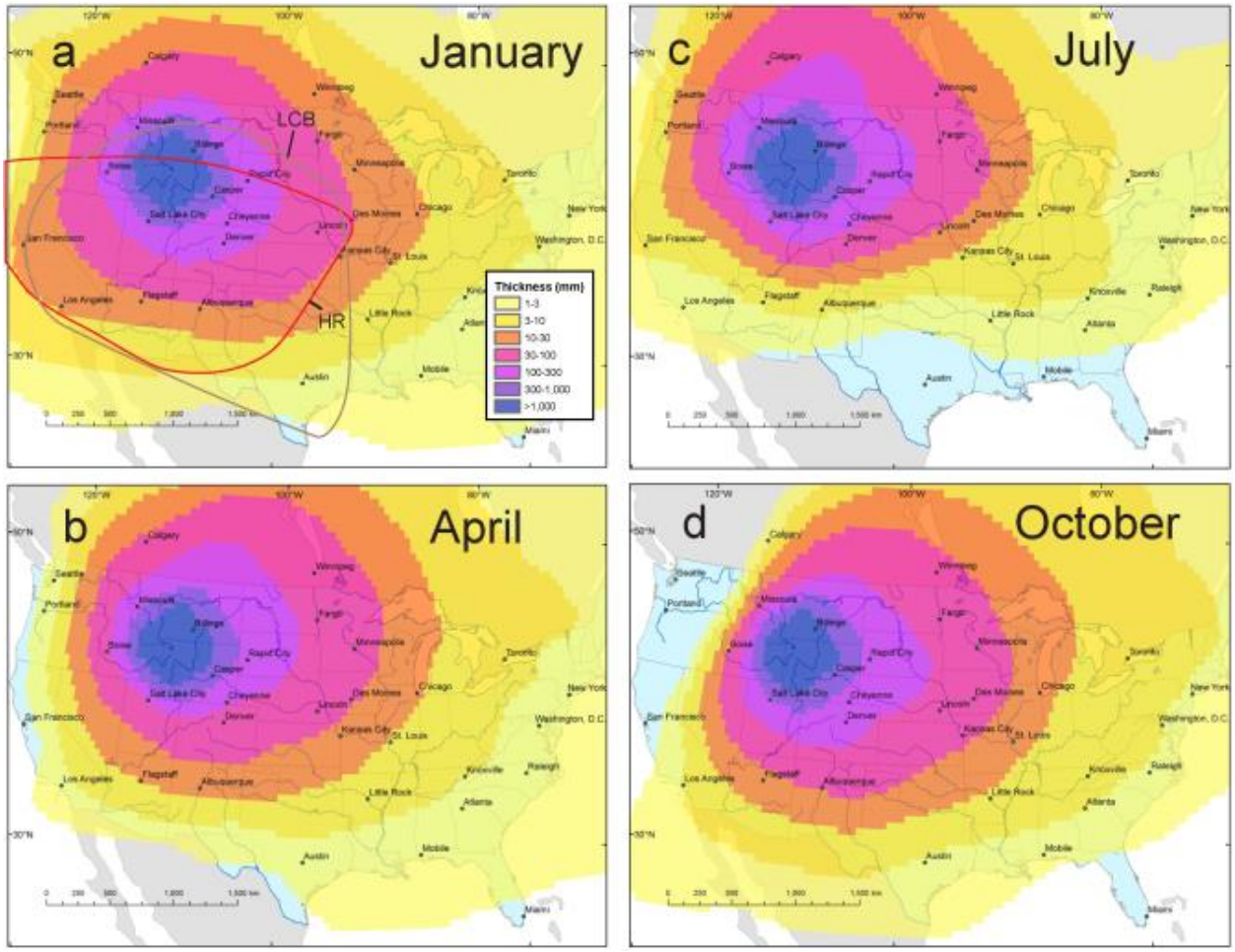

Figure 1.3: Yellowstone Ash Fall Models

Figure taken from Mastin et. al. (2014) demonstrating the model results for ash fall from a Yellowstone supereruption at varied times of the year: (a) January; (b) April; (c) July; (d) October. Figure (a) illustrates a bold red line which defines the Huckleberry Ridge Tuff Bed and the brown line as the Lava Creek B Tuff.

Previous studies have noted that ash from previous supereruptions of Yellowstone volcano had a far-reaching potential throughout the United States and Canada. With this information, a model of a hazardous map was created to inform the public of the potential damage zone they may live in, see Figure 1.3. (Mastin, Van Eaton, & Lowenstern, 2014) Though, scientists with extensive knowledge of the Yellowstone region point out that previous eruptions did not lead to any previously acknowledged extinctions. But significant damage would be expected with a supereruption, the largest damage would come from the ash plume and gases released into the atmosphere. Though, climatologist have also suggested that these

atmospheric pollutants may not diffuse to global proportions due to the volcano's northern land-locked longitudinal position that favors smaller scale westerlies wind patterns.

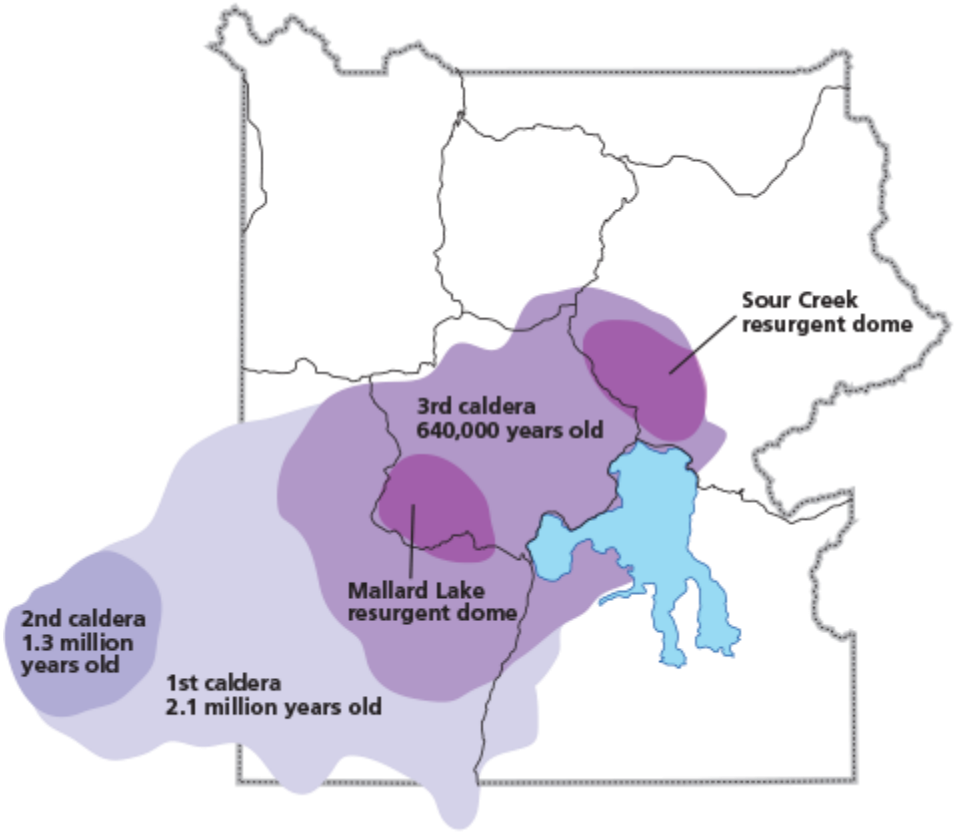

Figure 1.4: Map of Yellowstone Calderas

Figure taken from Yellowstone NPS Volcano website which is adapted from Smith & Siegel, 2000. (National Park Service 2017) Highlighted are the three most recent calderas formed by supereruptions of the Yellowstone Volcano.

There are three notable most recent supereruptions in the history of Yellowstone. The first occurred approximately 2.1 million years ago with the remnant caldera southwest of this region as seen in Figure 1.4. This eruption formed the 80 by 65 km Island Park Caldera and is the source of the Huckleberry Ridge Tuff formation. The ash and debris ejected form this event has been recorded to measure approximately 2500km^3 with traces found as far as Southern California. Another supereruption dated 1.3 million years ago created the 29 by 37 km Henry's Fork Caldera that is housed inside the Island Park Caldera. The eruption is the source of the Mesa Falls Tuff formation resulting from 250km^3 ejecta. The most recent supereruption took

place approximately 640,000 years ago, forming the Yellowstone Caldera and the source for the Lava Creek Tuff. The eruption ejected 1,000km^3 of ejecta and formed the 55 by 72 km caldera. The Yellowstone caldera rests atop the northwest portion of the Island Park Caldera. Yellowstone volcano does also have smaller intermittent eruptions between supereruptions that release magma flows at much smaller quantities and absent of violent eruptions.

Plate Tectonics

Extensive studies of the varying geological formations and seismic events from past and present in the region have garnered theories of Yellowstone's origins as largely attributed to the Laramide orogeny that began 70 to 80 million years ago in the Late Cretaceous, and ended in the late Eocene approximately 35 million years ago. (Camp, et. al., 2015) This mountain building event created the Great Basin and Range of the North American continent and primarily resulted from flat slab subduction of the Farallon and Kula plates along the U.S. Pacific coast. (Parsons, 1994) The large tectonic subduction of this plate millions of years ago punctured its way through the lithosphere and asthenosphere of the earth's crust. One paper states that ~15Ma a tear in the center of the downgoing slab formed from accumulated subslab pressure gradient and the weak strength of the young slab that does not hold up to the upwelling plume head. (Lijun and Stegman, 2011) In another paper by the same authors they state that the buoyant plume head alone does not cause the slab to break earlier (Lijun and Stegman, 2012). The model seen in Figure 1.5, taken from (Leonard and Liu, 2016) suggest that the only way the plume reaches near the surface is from a break in the slab, since the slab has overall larger volume therefore, portions of the plume would subduct with the slab rather than ascend by its own buoyancy.

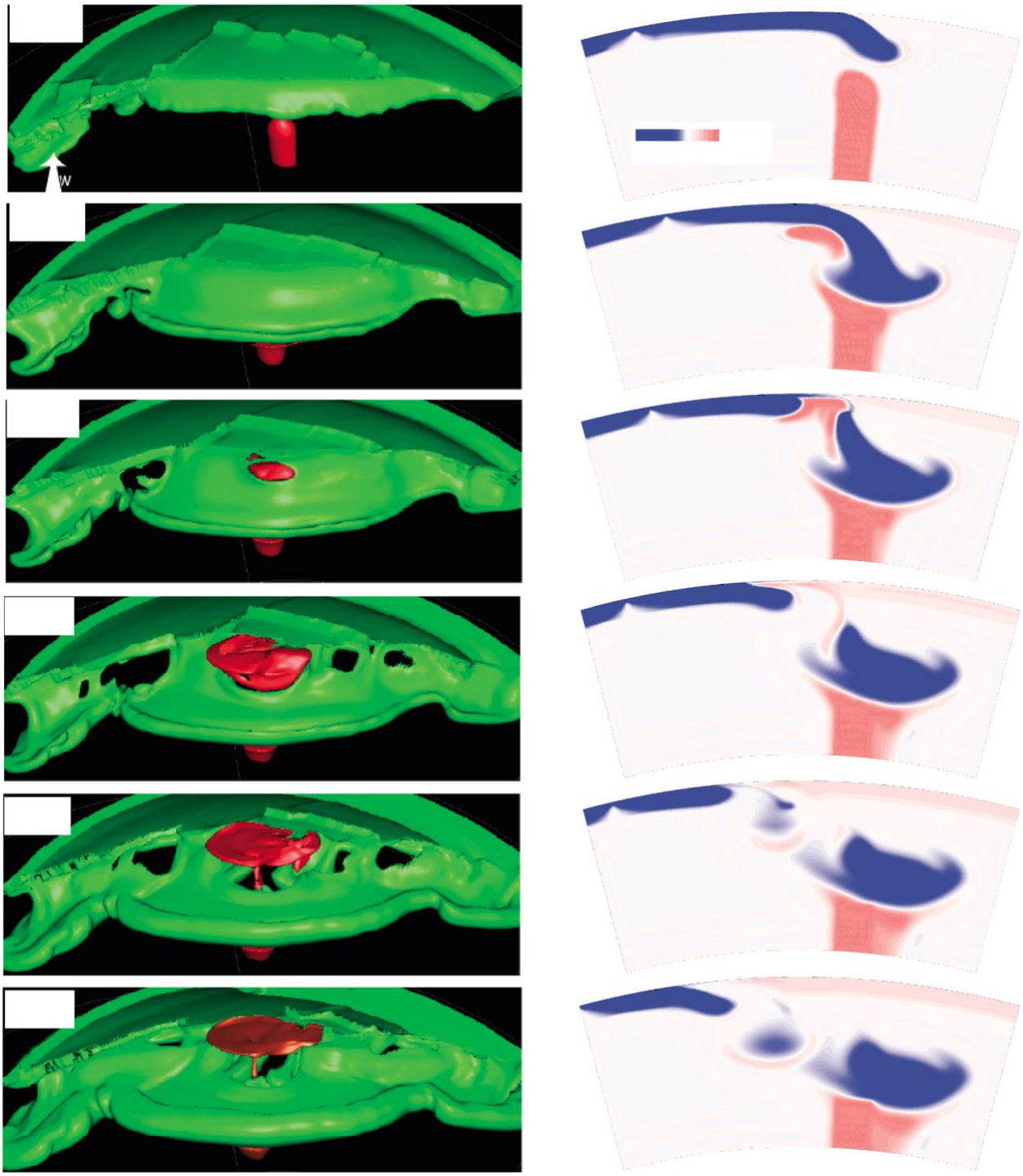

Figure 1.5: Farallon Plate Crossing the Path of a Plume

Figure taken from (Leonard and Liu 2016) displaying the (a) slab (green) and plume (red) interacting and (b) the progression of a subducting slab over a plume.

Geysers

In the Upper Geyser Basin, there are several mudpots, springs, pools and geysers. Most of the geysers are situated northwest of OFG. The geysers here are: Beehive, Castle, Grand, Economic, Oblong, Giant, Grotto, Lion and Riverside just to name a few. These features and OFG are all closely situated near the Firehole River, the main source of water that feeds the hydrothermal features. Old Faithful Geyser sets itself apart from the other geysers in this area because its waters are not interconnected to any other geyser features affording the predictability between eruptions. The other geysers share the same underground water conduit which cannot always provide similar predictable eruptions because, when one geyser erupts it may remove reservoir waters from other geysers (Bryan and Whittlesey 2008). Beehive Geyser and Depression geyser may be of interest for this study due to their very close proximity to a node (Number 029) with interesting signals.

Beehive geyser is cone geyser in close proximity to OFG and erupts 1 to 2 times a day. This geyser also has large eruptions with water and steam ejected to heights of 150 to 200 feet. And like many of the geysers here it too undergoes eruption fluctuations that are difficult to explain. One instance of erratic activity occurred in 2005 when the intervals between 1 day moved to a few weeks long intervals but then reverted to daily eruptions back in 2008 (Bryan and Whittlesey 2008). Figure 1.6 represents a cross-section of the geyser's inner mechanisms and a photograph of an eruption which best demonstrates the scale of Beehive geyser eruptions.

Depression geyser at first glance appears to be like one of the many pools in the Upper Geyser Basin, but it actually has small frequent eruptions. A fountain geyser that only erupts to heights of 4-10 feet while lasting about 5 minutes as the waters in the pool diminish but eventually refills after approximately 90 minutes (National Park Service, 2016). During the timeframe of the 2015 deployment, there were only three recorded eruptions during that time (National Park Service, 2016). Although signals recorded on Node 029 are more frequent (about every hour) there does not seem to be enough information regarding the subsurface conduit system for this geyser that could possibly be the source of these frequent signals.

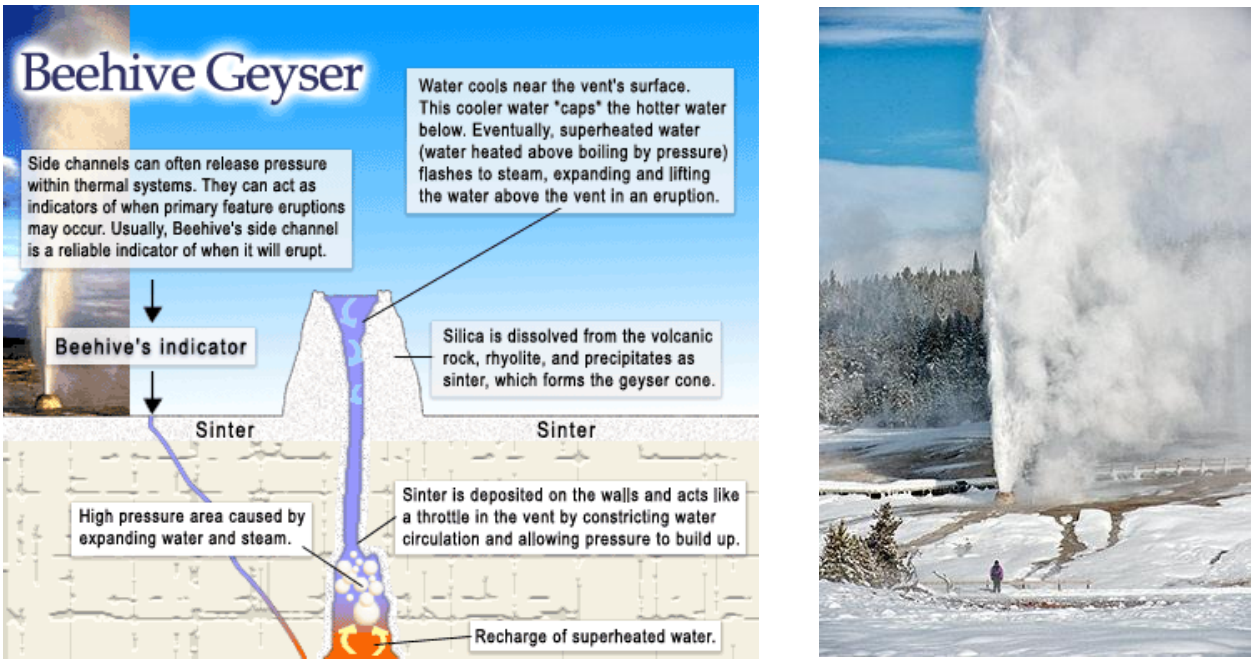

Figure 1.6: Beehive Geyser

The illustration on the left provides a succinct description of beehive geyser's dynamics (Yellowstone National Park (NPS), 2014). The picture on the right illustrates the magnitude of beehive geyser surface eruptions. (Picture taken from yellowstonepark.com (My Yellowstone Park Staff Writer, 2017))

Old Faithful Geyser has undergone observable changes in the last few decades. It was noted that prior to a large local earthquake of magnitude 7.5, the geyser eruption interval times used to be approximately every 64.91 minutes. Another significant earthquake in the region (Borah Peak, Idaho) measuring 7.3 in 1983 also disrupted the interval times and bringing eruption interval times to 78 minutes. By September 2007 an average of 90 minute intervals between eruptions became more common. (Bryan and Whittlesey 2008) The OFG has an East to West trending crevace opening with widening gaps at depth as inferred by observations from a video camera probe lowered into OFG in 1984, 1992 and 1993 as seen in Figure 1.7A (Hutchinson, Westphal and Keiffer 1997). Figure 1.7B showcases a deeper look into the active OFG as a "tea-kettle" environment that pushes waters from a large side chamber into the conduit ulitmately reaching the surface. Other details about the OFG are also mentioned in the *Introduction* of this paper.

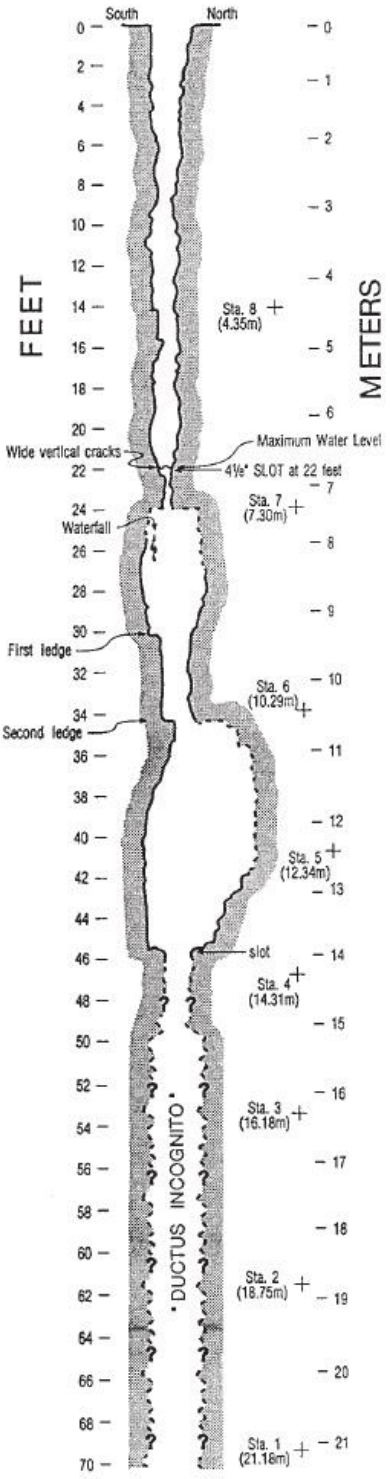

A)

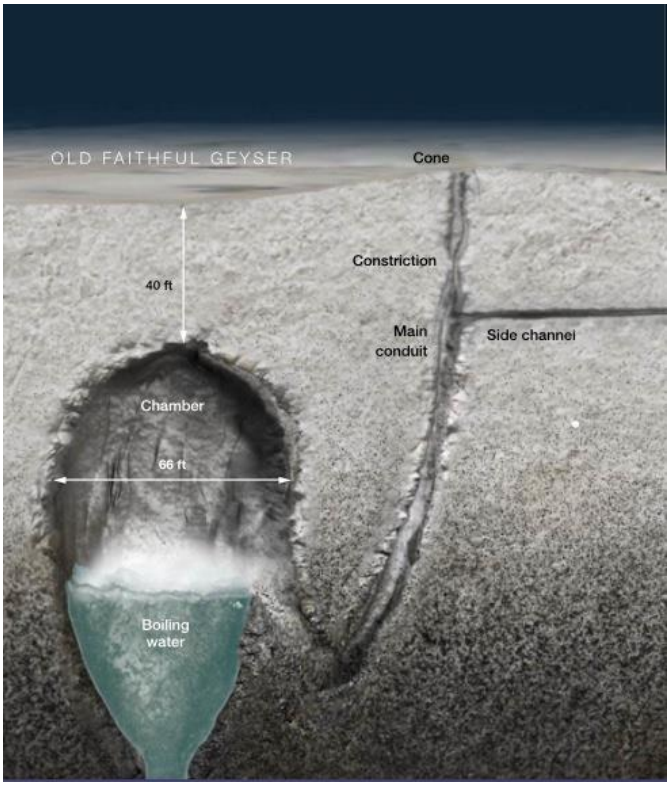

B)

Figure 1.7A: Shape of OFG Conduit

This figure was recreated from observations of video probes inserted into OFG. (Hutchinsen, et. al., 1997)

Figure 1.7B: OFG Conduit and Chamber

This figure taken from a National Geographic special animation showcasing Yellowstone geothermal and hydrothermal features is the latest version of OFG subsurface dynamic elements. (National Geographic, 2017)

Historical Seismicity

The Yellowstone region has continual seismic activity with most earthquakes registering as lower magnitude events, usually local (M_L) or moment magnitudes (M_W) below four. One notable event occurred on August 17, 1959, a 7.5M_L followed by five large aftershocks measuring 5.5 to 6.3 on the Richter scale within a span of ten hours (*see Figure A)*. There were 370 more aftershocks recoded four days later. (Smith and Siegel, 2000). As seen in Figure A, Hebgen Lake Fault, the culprit of the event caused landslides, an 8-mile fault scarp and, reports of 20-foot tsunami waves at Hebgen Lake. (Smith and Siegel, 2000) Five years later in October 1964, another earthquake speculated to have been a 5.3M_L again hit the region which, Smith and Siegel claim is an aftershock from the 7.5 earthquake years before. The events prompted further extensive seismic investigation at Yellowstone.

The University of Utah established a website with "live" viewing of data received from their broadband seismometers placed around the park along with a release of quarterly reports describing seismic activity in the region (Farrell, Burlacu and Roberson, 2015) . As mentioned before, many of the earthquakes in the area are smaller magnitude with swarms seen frequently throughout the region. Although monitoring is intensive, since most of the current stations are mostly higher frequency range; it can be difficult to record micro- seismic events that are not immediately surrounding the stations. The 133-nodal array of high frequency instruments might assist with magnifying events that would otherwise be overlooked by the permanent stations. One of the main reasons for closely monitoring Yellowstone seismicity is the ability to find a pattern that could be a pre-cursor to possible eruptions in the future as the same forms of monitoring exist at other volcanic regions.

Chapter 2: Experiment Geometry & Equipment

For this investigation, the temporary deployment of 133 Fairfield Z-Land 5-Hz, 3-component geophones were installed in concentric circular pattern in the Upper Geyser Basin (Figure 4) during the first two weeks of November 2015. The average station spacing in the array was ~50 m, and the aperture was ~1 km. This array created a unique opportunity to probe crustal and lithospheric structure by examining recordings of various seismic phases from passive local seismic events. Differences in phase travel times on the densely-spaced stations may aid in identifying high resolution subsurface plumbing of the geysers and the structures that surround them. Figure 2.1 details the setup of the nodes around the Upper Geyser Basin with OFG as the focal point of the array.

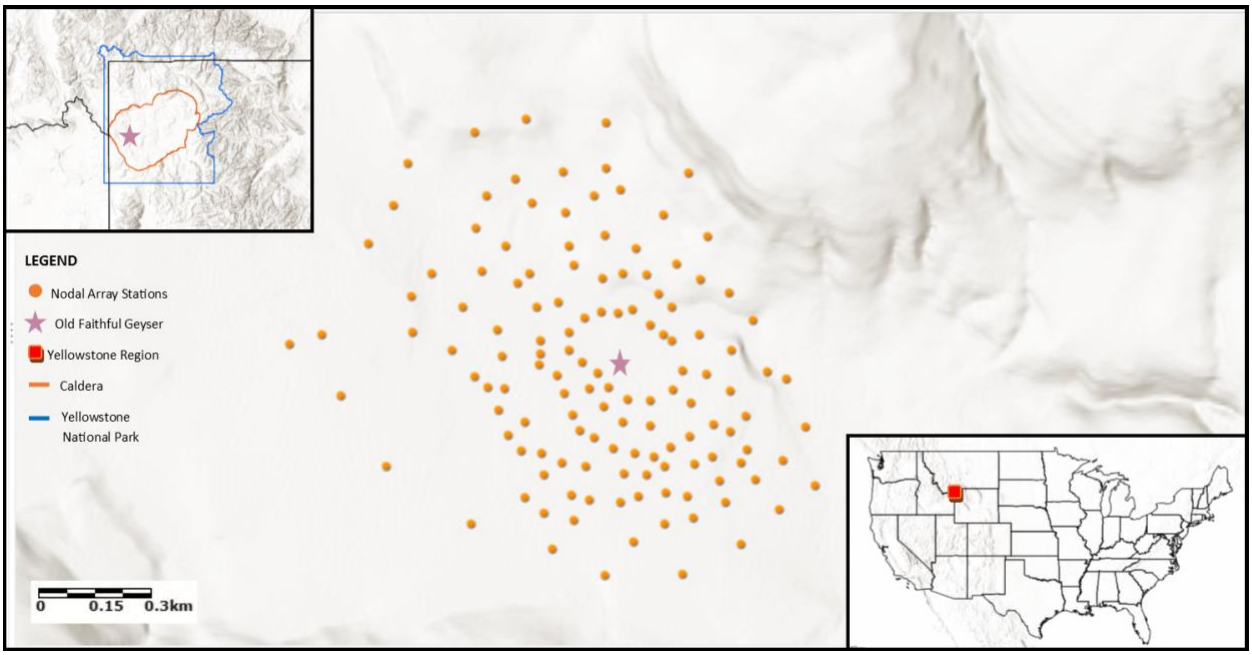

Figure 2.1: Map of Nodal Array arrangement around OFG

The permanent seismic network (WY) at Yellowstone National Park consists of broadband and geophone seismometers. The station located by Old Faithful (YFT) contains two

different brand and frequency seismometers. The first is a Trillium Compact Broadband seismometer 20s version that is a high broadband, high gain seismometer recording on all 3-channel components with a frequency response flat to velocity from 20 seconds to 100Hz. The second instrument, a Mark Products L-4C with extremely short period response band, high broadband recording one single channel in the Z (vertical) component. Both of these seismometers have a sample rate of ≥ 80Hz. Data collected from these stations will be utilized more as a verification of events to be used for analysis.

The temporary deployment used 133 Fairfield Nodal Z-Land 3C geophones that lie in the spectrum of very high broadband and will attenuate lower frequencies. For further reference of the nodal array arrangement, a map with the station numbers is provided in the *Appendix* of this document.

Chapter 3: Methods

For the first potion of this study, local seismic sources identified by the current Yellowstone broadband network were identified on each nodal station. Each nodal station depending on its distance from the source comprised a different time arrival, with some containing time arrival diversity only in the milliseconds. This is due to the array's condensed placement. In order to identify specific seismic signals, the Z-channel which is the vertical component of the nodal station, stood as the best in aiding with picking first arrivals (P-waves), and any discernable arrivals of S-waves, reflections, refractions and any surface waves. The identification of noticeable signals come mostly from "hand-picking" using Seismic Analysis Code (SAC) software. The incredibly heterogeneous medium of the subsurface here in this region makes it a bit difficult to apply velocity models like the iasp91 as it is more suited for somewhat evenly layered stratigraphic regions without magma plumes in the path.

Upon initial observations of the data and trying to find signals within the noisy data seemed impossible at first but became more streamlined once signal processing helped in finding ways to separate the noise from the signals. One of the first processes I used was time-domain spectral imaging which best represented the varying frequencies contained within the digital data during a specified time range and can be seen in the *Results & Discussion* section for events picked up by the array. Knowing frequency ranges contained within the data aided with the separation of the different types of signal that occurred during that time-frame, such as, geyser water temperature increase before an eruption and coincidentally any fracturing caused by the waters movement and pressure on surrounding rock. Noting lower frequencies for teleseismic earthquakes was also present in the spectral data. This also proved that although response threshold for the nodes are higher frequency response the clear visibility of identifying distant earthquakes normally seen at much smaller frequencies were indeed evident in the node data. A recent paper by Farrell et. al. (2015) revealed a large event, low P-wave velocity body, interpreted to be the crustal magma reservoir via 3-dimensional plots. SAC provided the products

for the signal processing in the experiment and the outcomes are thoroughly discussed in the *Results & Discussion* section.

The second segment of the study incorporated ground motion visualizations (GMV) using Matlab scripts created by IRIS (Trabant, et. al., 2012). The GMV's are an animated visual of earthquake wave energy as it propagates through each nodal station through a timed analysis of each different wave phase arrival. Close examination of the data in order to find arrivals of body waves such as P and S waves, in addition to, arrival of regional phases such as pP, and sP waves that may occur from smaller magnitude earthquake events are a primary research stage. Even though, most of the lithologies in the region consist of igneous rocks and expected velocities for first arrivals would range above 4500 m/s the GMV showed a fluctuating arrival time for different wave phases in certain areas of the array. These observations are detailed in the *Results & Discussion* chapter.

Chapter 4: Data

The data obtained by the array established a total of eleven days' worth of usable data. The installation and recovery dates did not include viable data. A viewing of the data showed a high noise-to-signal ratio for the stations located at closest proximity to geysers, most notably stations neighboring OFG. Initial investigation involved a comparison of node data to events recognized by permanent broadband stations in the area, as well as, comparing geyser tremor signatures with recorded eruption times.

Below are detailed seismogram images of earthquake and geyser signals recognized by the array. One other interesting finding in the data was a tremor caused by bubble collapses similar to results by Kedar and Kanamori (1998).

Raw Data

This section showcases the raw data before applying pre-processing methods and filters. In figure 4.1, stations 004, 005, 017, 022 illustrate the cyclical signatures seen throughout a normal day at stations located close to the geyser. The data is from November 11th around the same time frame that the 6.5Mw Aleutian Islands (Atka, Alaska) earthquake occurred.

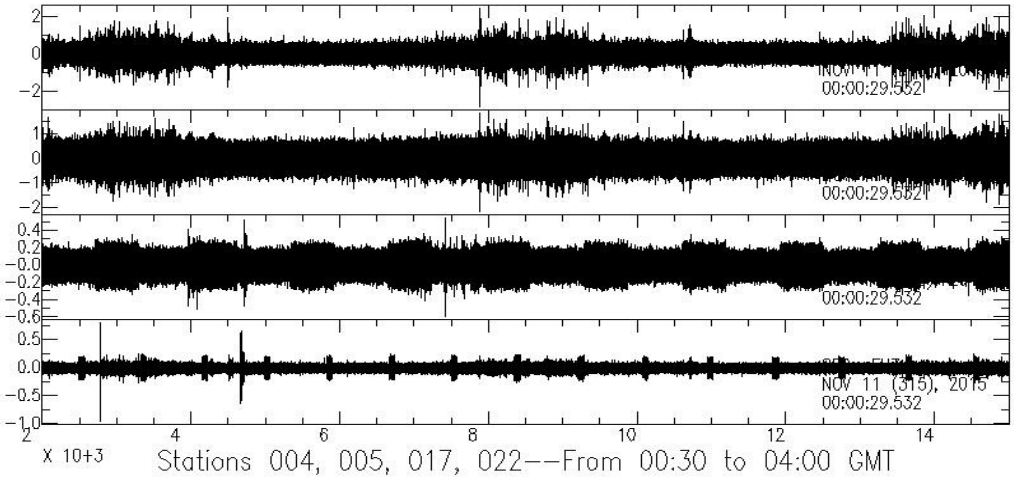

Figure 4.1: Raw data of stations near OFG
Seismograms for stations 004, 005, 017 and 022 on November 11th with a timeline of 3.5 hours. The x-axis is time in seconds and the y-axis is counts in revolutions.

Earthquake Data

In order to get better results of the earthquake signals, a removal of the instrument response helped to identify signals much faster by eliminating a lot of the noise present in the data. This process in SAC involves using the TRANSFER command to remove the instrument response by deconvolution using spectral division from selected corner frequencies. The detailed seismic convolutional model (Robinson, et. al., 1986) detailed as;

$$x(k) = c(k) * w(k) + n(k)$$

where, ***k*** = *integer-valued time index*
x(k) = *received seismic trace*
c(k) = *reflectivity function (i.e., the sequence of reflection coefficients representing the desired lithology)*
w(k) = *seismic wavelet (including source effects, absorption, multiple-reflection effects, and receiver effects)*
n(k) = *additive noise (which generally can be made small by the use of good field techniques)*

Figure 4.2 shows filtered results of a 2.5M_L earthquake approximately 100km southwest from the array and the permanent station YFT. The precise epicenter lies at 43.569 latitude and -110.389 longitude and occurred at 17:51:20 GMT. Figure 4.3 is an image of a teleseismic earthquake that occurred off the coast the Atka Islands in Alaska which is part of the Aleutian Islands chain. The earthquake registered as a 6.5MW at 16:03:46 GMT with an epicenter of 51.639 latitude and -173.0746 longitude and 15km depth hypocenter. Figure 4.4 are the traces of two teleseismic events roughly one hour apart that occurred off the coast of Coquimbo, Chile. Both events were documented as 6.9M_W events as picked up by both the array and YFT station. The first occurred at 01:54:38 GMT with a 12km depth origination and epicenter of -29.507 latitude and -72.007 longitude. The second event had a 10km depth hypocenter and -29.5097 latitude and -72.0585 longitude epicenter which occurred at 02:46:19 GMT.

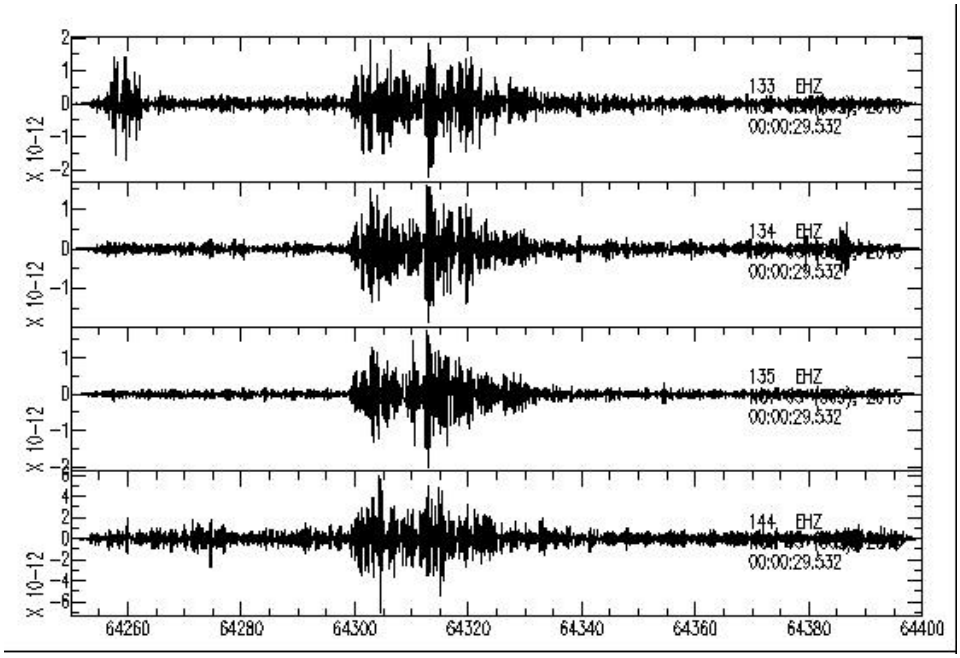

Figure 4.2: Seismic traces of 2.5M_L Wyoming Earthquake

Shown from top to bottom are stations 133, 134, 135, and 144 which are located farthest East of the array. The x-axis is in seconds which measures from 17:51:00 to 17:53:50 and the y-axis is in counts. These traces represent the signal after instrument response was removed and a bandpass Butterworth filter with corner frequencies of 1.5 to 4.5Hz.

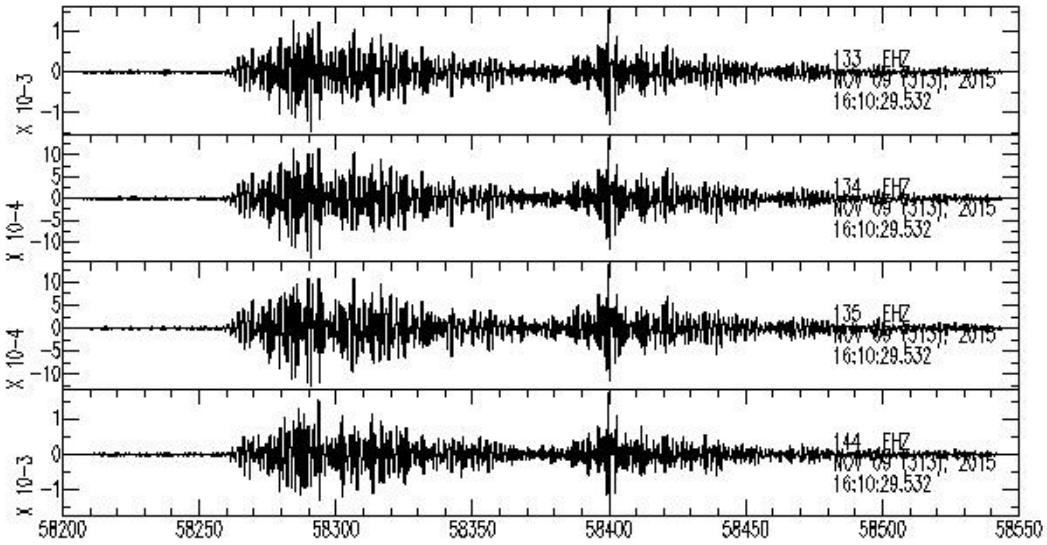

Figure 4.3: Seismic traces of 6.5M_W Aleutian Islands Earthquake

Shown from top to bottom are stations 133, 134, 135, and 144 which are located farthest East of the array. The x-axis is in seconds which measures from 16:10:29 to 16:15:29 and the y-axis is in counts. These traces represent the signal after instrument response was removed and a bandpass Butterworth filter with corner frequencies of 1.5 to 4.5Hz.

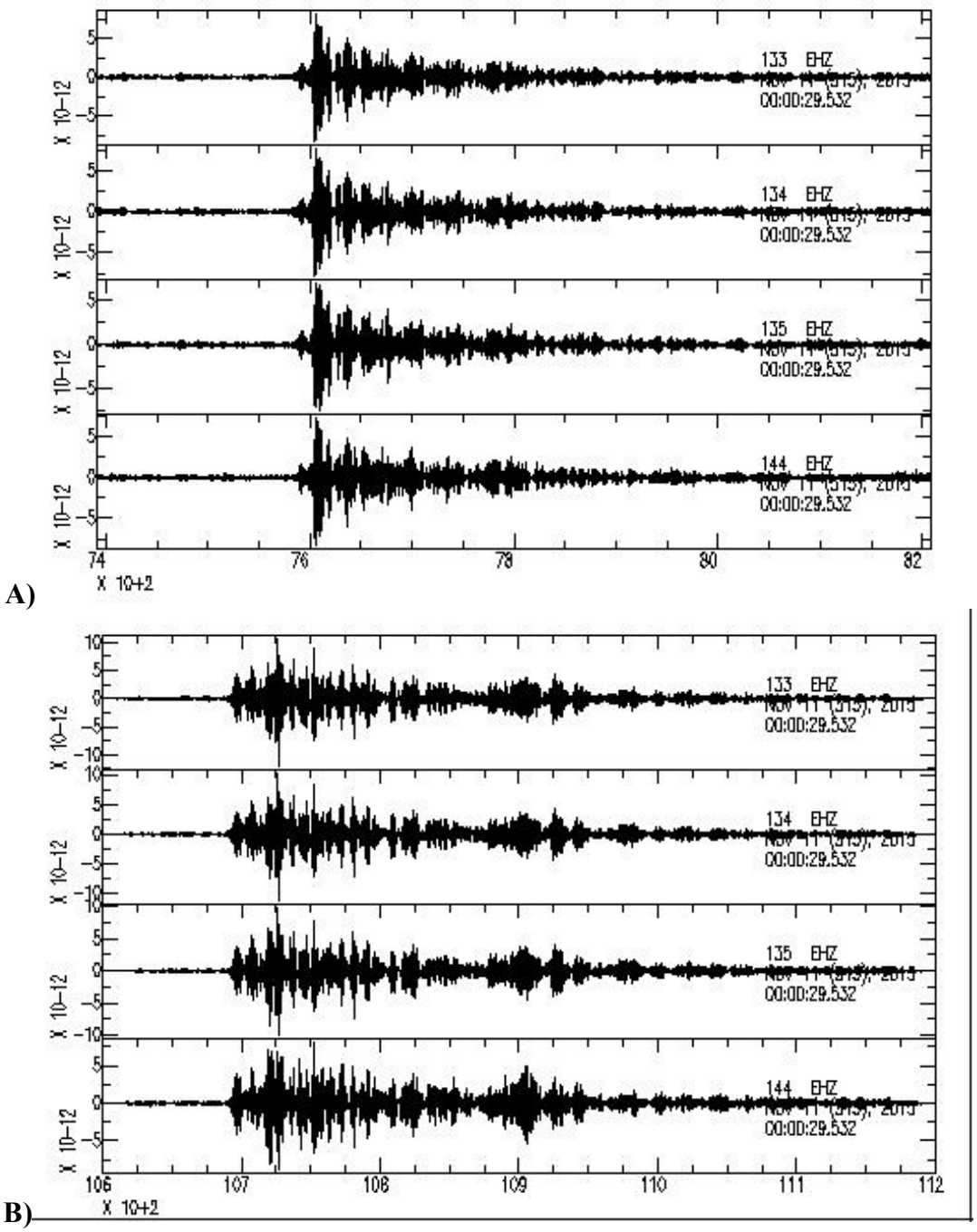

Figure 4.4: Seismic traces of 6.5Mw Aleutian Islands Earthquake

Shown from top to bottom are stations 133, 134, 135, and 144 which are located farthest East of the array. The x-axis is in seconds and the y-axis is in counts. A) Is the first teleseismic event that occurred off the coast of Chile with time range of 02:03:49 to 02:07:08 GMT. B) Are traces for the second earthquake that occurred off the coast of Chile with a time range from 02:57:09 to 03:07:09 GMT. These traces represent the signal after instrument response was removed and a bandpass Butterworth filter with corner frequencies of 0.5 to 1.5Hz.

Geyser Data

In looking at the seismograms it became apparent that there were several signals from more than one hydrothermal feature. The signals that were best attributed to geyser or pool bubbling was also concentrated to very local areas of the array and difficult to pinpoint the specific source. Station 029 as mentioned before demonstrated signals with consistent patterns throughout much of the day. The likelihood of these signals associated to a geyser are very likely but, pinpointing which one in particular is another task all its own as much of the activity is suspected to be primarily underground without any significant signs at the surface. Figure 4.5 shows raw data for station 29 at 250 samples per second for dates Nov 3rd, 6th, 7th, 8th, 10th, 12th, and 13th.

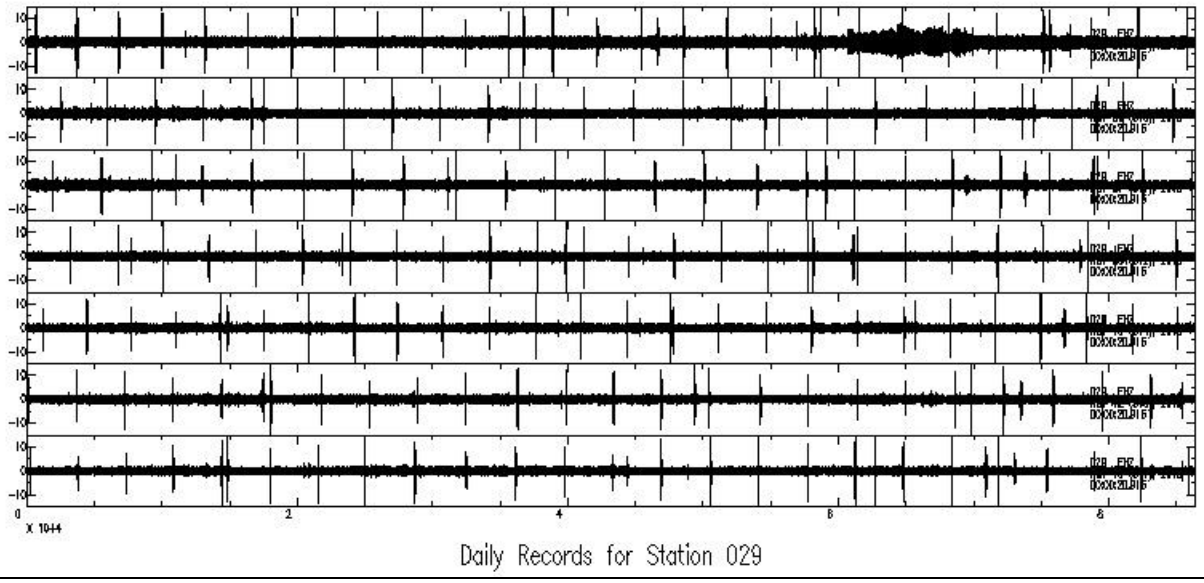

Figure 4.5: Seismic traces of Geyser Sources for Station 029
Shown are 24-hour period raw seismograms for station 029. The x-axis is in seconds and the y-axis is in counts.

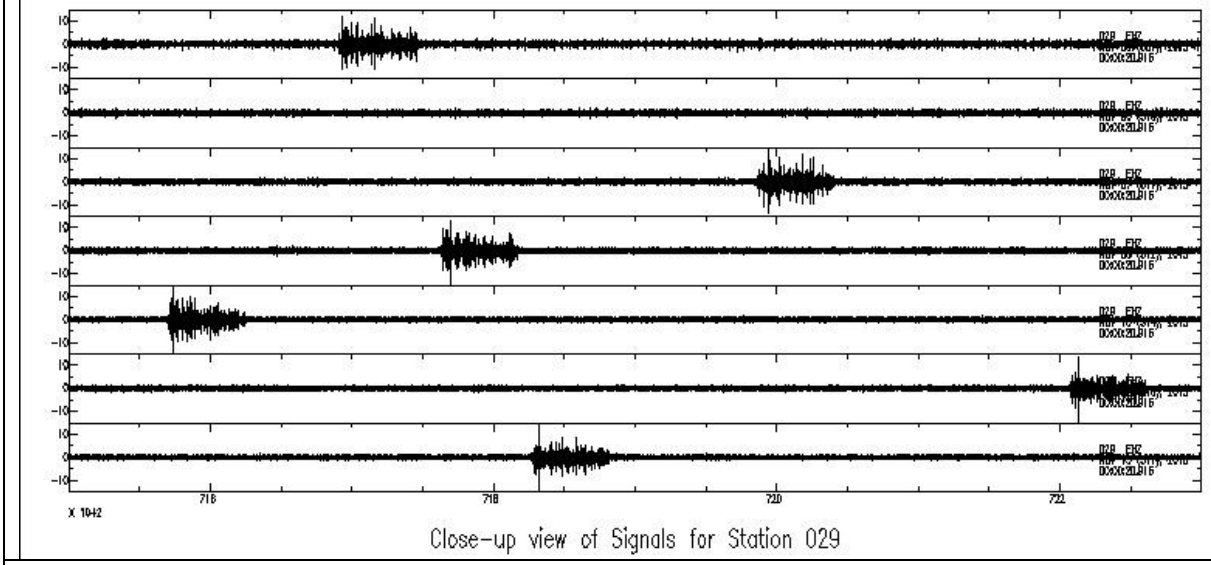

Figure 4.6: Close-Up Seismic traces of Geyser Sources for Station 029

Shown are zoomed in raw seismograms for station 029 from 19:52:00 to 20:05:20. The x-axis is in seconds and the y-axis is in counts.

Suspected Mine Explosions

The array also seems to have picked up what could be mine explosions in East Wyoming centered at a coal mine. There were two events recorded by permanent stations: 1) 3.1M_L at 0km depth at 22:03:41 UTC with latitude 43.8163 and longitude -105.3856 and 2) 3.4M_L at 0km depth at 22:05:50 UTC with latitude 43.6541 and longitude -105.2043. Looking at these coordinates on Google Earth the epicenter is located at the Thunder Basin Coal Company that appears to be an open-pit mine. There is more detail regarding this event in the Results section under the GMV results.

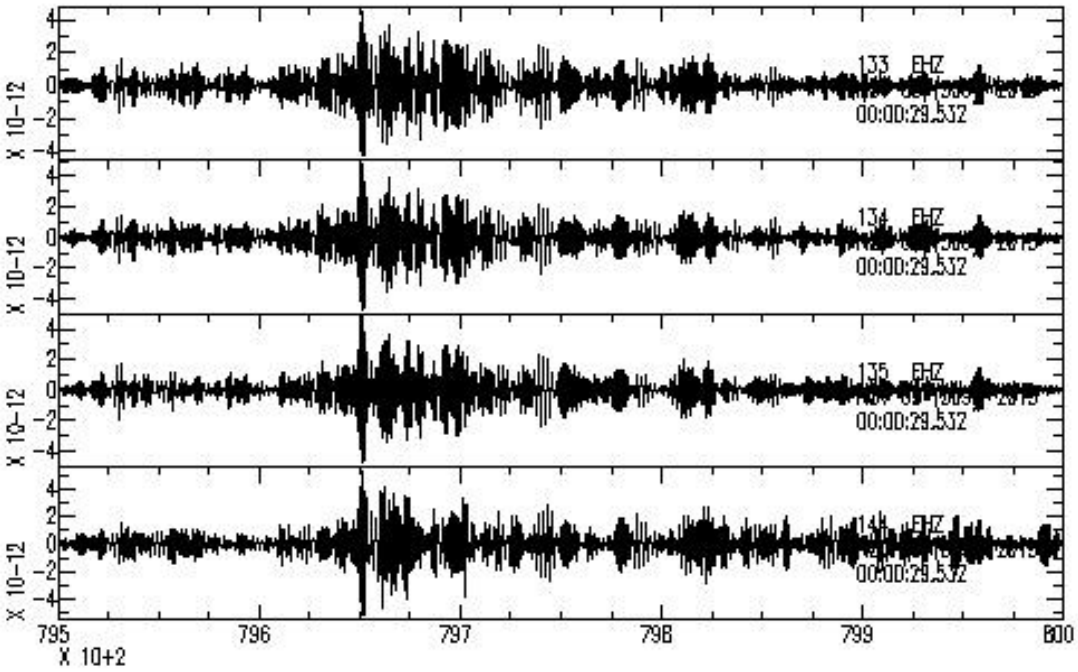

Figure 4.7: Seismic traces of suspected Mine Explosions

Shown from top to bottom are stations 133, 134, 135, and 144 which are located farthest East of the array. The x-axis is in seconds and the y-axis is in counts. These traces represent the explosion signal after instrument response was removed and a bandpass Butterworth filter with corner frequencies of 0.4 to 0.8s.

Chapter 5: Results & Discussion

Ground Motion Visualizations

A Matlab script available from IRIS allowed us to create animations displaying wave propagations from seismic sources that are captured in series to create a time series "movie." The original script was created with an older version of Matlab that needed to be updated to use with newer versions of the software. The script called several other function files, such as, Java libraries for TauP time estimation of varied wave phase arrivals. The global velocity model "iasp91" was also incorporated in the script to help determine time of different phase arrivals. Though, some of the phases seemed to be identified incorrectly as you may be able to see in the following section of these observations. It is unclear if the arrivals were not correctly identified due to filtering choices or the extreme heterogeneity of the subsurface medium. As discussed in the background, much of the subsurface in this area is highly fractured with most of these fractures holding water reservoirs that feed many of the hydrothermal features in the area.

In looking at these animation observations, it is clear that there appears to be changes in velocities in certain areas of the array. When playing the GMV movies for some of the events at different speeds some of these changes are visible when amplitudes of the signal are smaller. The observations of varying signal arrivals are from northeast to southwest, where arrivals seem to arrive first on the northeast quadrant of the array and delayed arrivals in the southwest quadrant of the array. In the tables of observations to follow the description of "clockwise rotation" will often refer to the changing velocities seen in the northwest and southwest quadrants of the array.

The GMV observations for the 6.5Mw Atka Islands, Alaska (Aleutian Islands expanse) displayed well with first arrivals homogenously traveling through the array. Though, as some of the amplitudes of the signal shrink a rotation of the wave arrivals occurs. As mentioned before, this is an indication of slowed velocities in the southwest quadrant of the array. The southeast quadrant of the array is the proposed location of the OFG water chamber mentioned in Chapter 1 that could be causing these slowing wave arrivals as well as the glacial sediment deposits.

Aleutian Islands 6.5Mw Earthquake Observations

Table 1: Atka, Alaska (Aleutian Islands) GMV Observations

TIME	OBSERVATION
	P-wave arrival arrives with slight dilitational downward signal from the southeast of the array.
	Waves arriving after initial P-wave appear to roll in from the northwest.
	Bandpass Butterworth – 0.05s - 1.5 Hz
16:11:14	Shift back to southeast arrivals with a clockwise "rotation"
16:11:19	Waves appear to roll-in UP from a southwest direction and continues to roll northward with waves propagating in a southeast direction
16:11:22-16:11:24	see a clock-wise rotation of wave propagation with slower arrivals on the southeast portion of the array.
16:11:30	Figure of three amplitudes (UP, DOWN, ZERO)
16:11:30	Waves appear to come-in from the northwest
16:11:4	Appearance of Southeast wave arrivals
16:11:43	Arrival of shear wave appears to arrive at the array. Propagation of different wave arrivals such as reflections refractions and diffractions are further apart appearing to be slower. (i.e. Reverse in polarity is time-wise further apart but could be due to larger amplitudes)
16:12:06	Amplitudes begin to shrink down and appearance of different wave arrivals speeds up.
16:12:16	Waves appear more dispersed direction of arrival is not all that discernable
00:02:00 (Elapsed Movie time)	elapsed visualization time the signals arrive with smaller amplitudes which cannot be seen well enough to discern wave arrivals. This could be due to a lowered magnification of amplitudes to try and attenuate noise.
16:13:16	Wave arrivals are more apparent as amplitudes increase with what seems to be surface wave arrivals.
16:13:29	Arrivals appear to come in to the array from an eastward direction. (This seems to occur at smaller amplitudes shortly proceeding a higher amplitude arrival.)

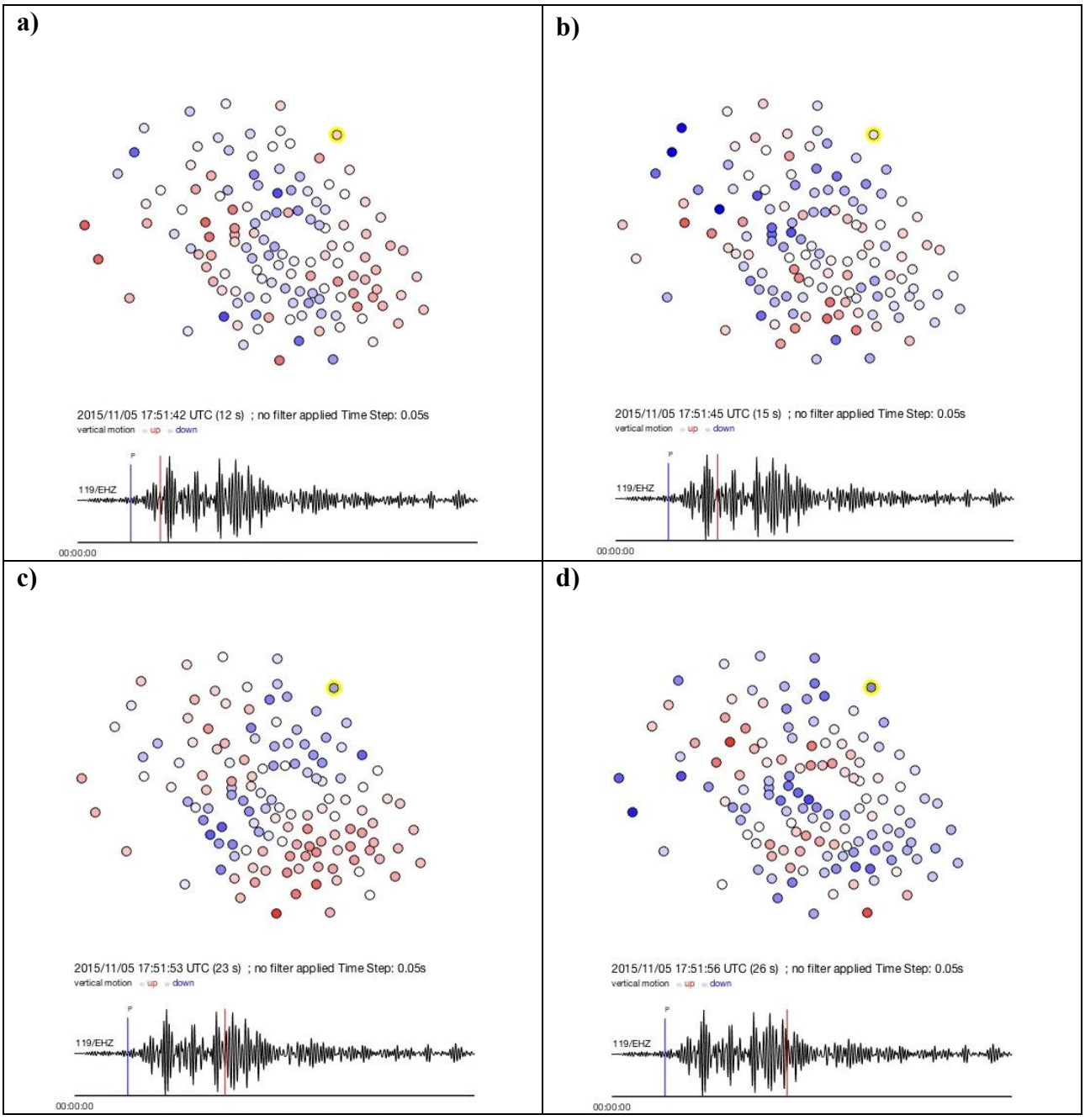

Figure 5.1: GMV screenshots of Aleutian Islands 6.5 M_W Earthquake

Screenshots of GMV with the seismogram for station 119; a) at 17:51:42 showing arrival just after P-wave arrival. b) Screenshot of non-uniform arrivals after high amplitude arrival. c) Uniform arrivals once again at 17:51:53 which appears to be shortly after the S-wave arrival. d) At 17:51:56 we see a time variation in arrivals once again after higher amplitudes.

Coquimbo, Chile 6.9Mw Earthquake Observations

Table 2: Chile Earthquake GMV Observations

TIME	OBSERVATION
	The stations are saturated from the very beginning of the file even before the arrival of earthquake signals
	Bandpass Butterworth filter 0.09 –0.9s
22:06:25	Signals come in with no noticeable change between dilatational (down) and extensional (up) movement within the same frame. Could indicate wavelengths at this time are longer
22:06:50	Waves also appear to come in from Northwest direction
22:06:55	Propagation of waves appear to have a counter clockwise rotation
22:06:57	Arrivals appear to come from westward direction
22:07:07	Waves appear to sway from northwest and immediately back
22:07:20	Waves appear less saturated at higher amplitudes. Phase shifts are also more discernable.
22:07:31	Arrivals appear to come from the southeast direction which is the correct direction from the earthquake epicenter.
22:07:55	Waves appear to come in from northeast direction

The Chile 6.9Mw earthquake GMV saturated the stations with the signal which can be seen by the complete blue (down) or red (up) motions. Once the amplitudes of the signal shrank, a shift between up and down became more apparent one frame at a time. The GMV for the Chile earthquakes did not suggest a change in velocities which could be the case due to its vertical arrival to the array that perhaps did not encounter a medium that would attenuate the signal significantly.

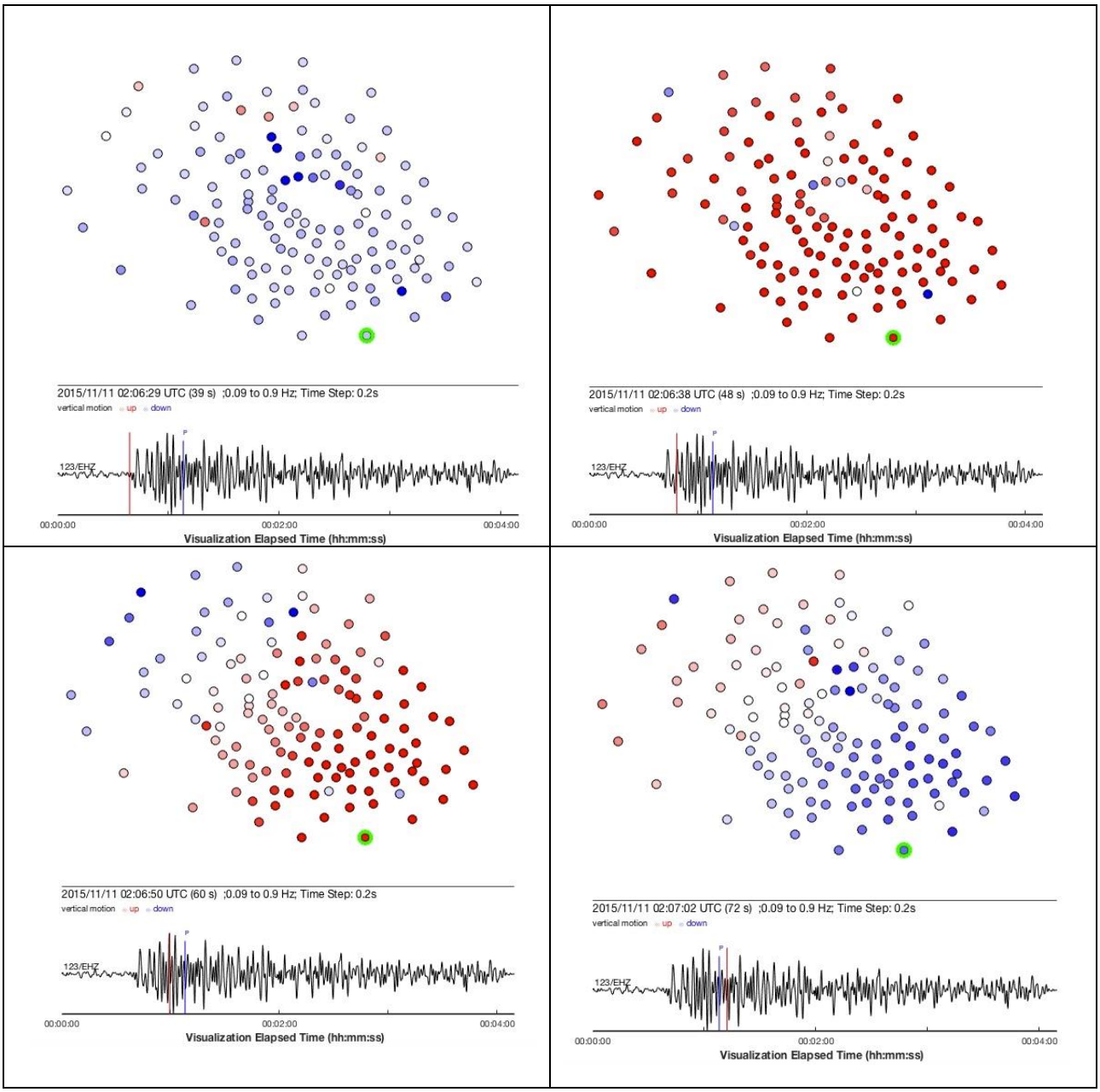

Figure 5.2: GMV screenshots of Chile 6.9 Mw Earthquake

Screenshot of GMV at 17:51:42 showing arrival just after P-wave arrival. b) Screenshot of non-uniform arrivals after high amplitude arrival. c) Uniform arrivals once again at 17:51:53 which appears to be shortly after the S-wave arrival. d) At 17:51:56 we see a time variation in arrivals once again after higher amplitudes.

South Wyoming 2.5M_L Earthquake Observations

Table 3: Local Earthquake GMV Observations

TIME	OBSERVATION
	First arrivals have uniform arrival times. Thereafter, waves come in a bit more scattered in the southwest portion of the array.
	Bandpass Butterworth filter – 1-3 Hz
17:51:52	arrivals become once again uniform
17:51:54	uniform arrivals
	Higher amplitudes noted on the seismogram correlate to uniform arrivals to the array as well as saturated signal arrival.
	Lower peak amplitudes show more attenuation throughout the array.
17:51:40	first arrival noted but appears very faintly
17:51:41	more noticeable waves arrive and saturate signal a bit more
17:51:42	wave arrivals appear to have less uniformity in their arrival to the array.
17:51:45	arrivals are again dispersed
17:51:56	arrivals are once again more scattered and less uniform

The GMV for the South Wyoming local earthquake actually showed more evidence of attenuation as the signals arrived to the array. The "rotation" effect can be seen more regularly as the signal moves through the array. This could be attributed to the idea that the local earthquake is located within 10° of the array that makes its travel through the highly fractured subsurface more prevalent.

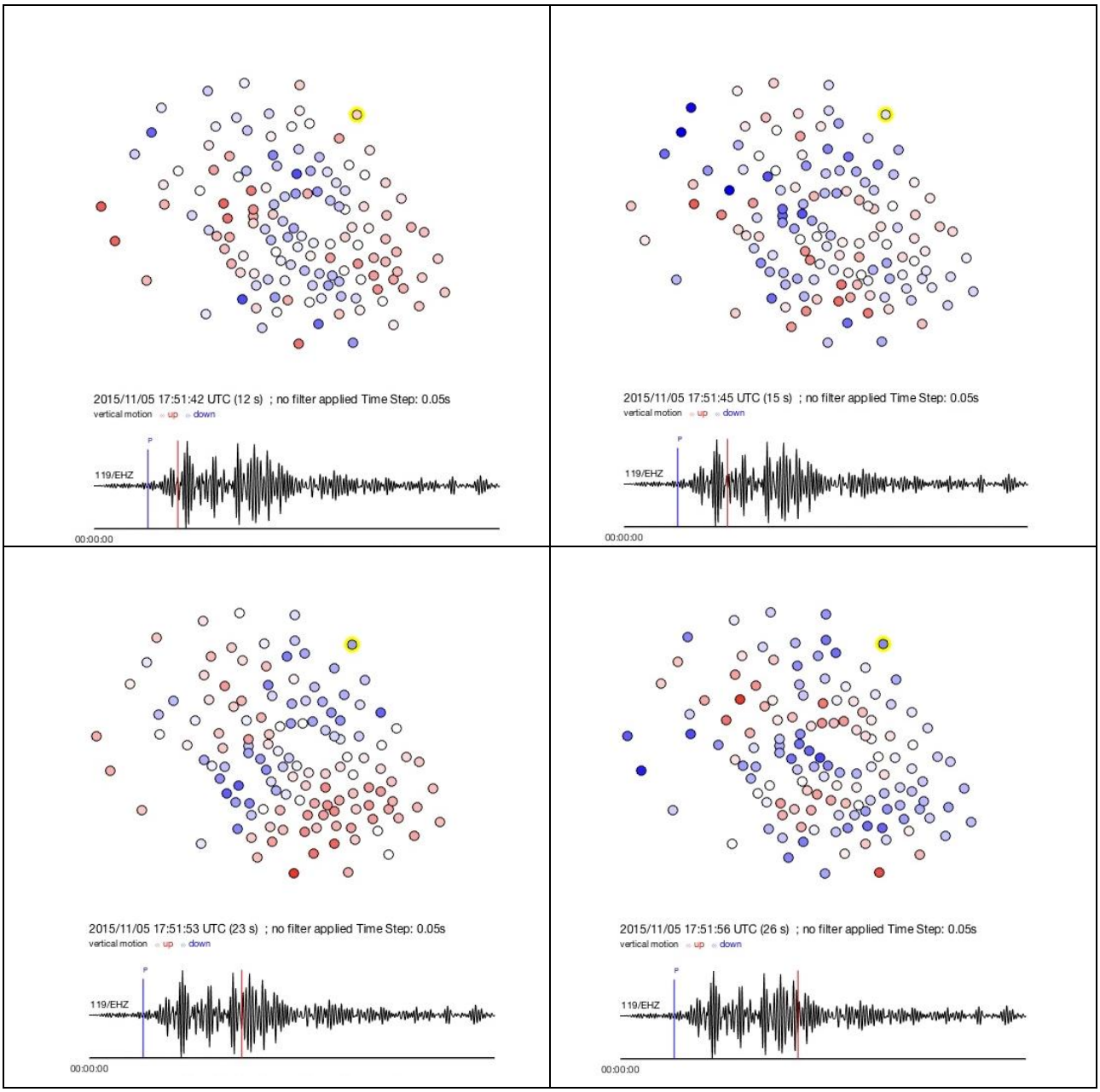

Figure 5.3: GMV screenshots of South Wyoming 2.5 M_L Earthquake

Screenshot of GMV at 17:51:42 showing arrival just after P-wave arrival. b) Screenshot of non-uniform arrivals after high amplitude arrival. c) Uniform arrivals once again at 17:51:53 which appears to be shortly after the S-wave arrival. d) At 17:51:56 we see a time variation in arrivals once again after higher amplitudes.

East Wyoming 3.4M_L Surface Explosion & Intermittent Geyser Observations

Table 4: Explosion and Geyser GMV Observations

TIME	OBSERVATION
	The GMV intermittently contains geyser signature that seems to radiate out from the center of OFG.
	Bandpass Butterworth filter 0.5 –1.5Hz
22:06:04	Waves appear to radiate out from OFG one blue and red cycle
22:06:28	Waves from first explosion at 22:03. The wave arrivals are very subtle and short. The first explosion measured a 3.1M_L. (Prior to script pick of P-wave arrival)
22:06:44	
22:08:04	Higher amplitudes allow for better visualization of waves rolling into the array.
22:09:02	Section between two larger amplitude arrivals, waves are still coming clearly from a southeast direction
22:09:06	Appearance of waves changing direction from easterly source. They appear to come from west and south directions.
22:09:29	Waves again appear more saturated and clear arrival from eastern direction.
22:10:06	Waves appear to come from a northeast direction
22:10:21	The nodes appear saturated from up or down signal for longer periods.
22:11:09	Waves appear to dissipate and can only see random geyser noise.

The GMV for the explosion that occurred in East Wyoming was much more drenched with local noise making wave arrivals harder to discern, especially for smaller amplitude arrivals. The attenuation seen is similar to the Aleutian Islands GMV where it appears that slower arrivals occur at the southwest quadrant and faster arrivals in the northeast quadrant of the array. There also appears to be minor local wave propagations from local geyser sources that seem to emanate from geyser hill.

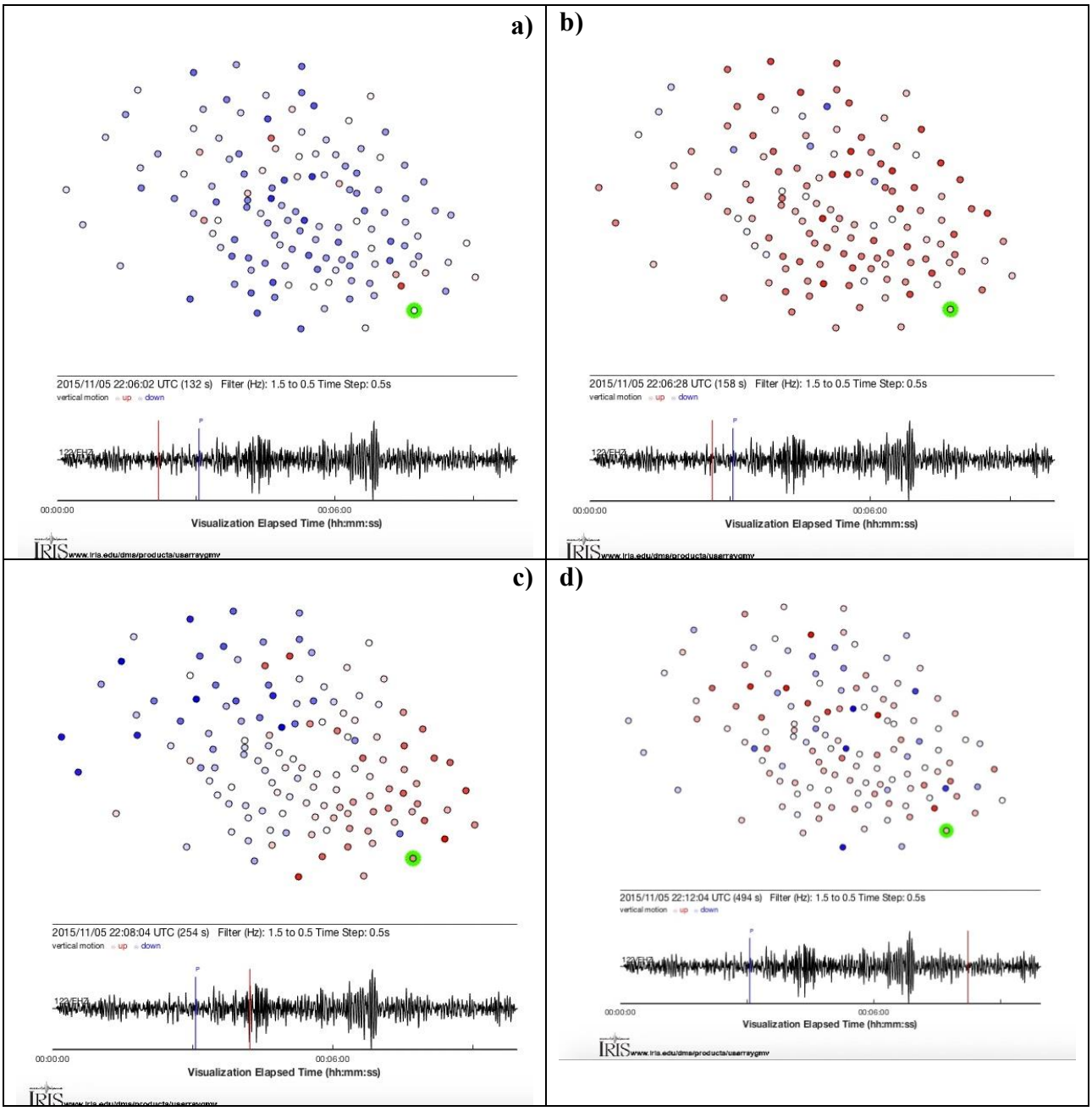

Figure 5.4: GMV screenshots of East Wyoming 3.4 M_L Earthquake (Explosion)

Screenshot of GMV at 22:06:04 showing what appears to be energy radiating out from the center of the array. b) Screenshot of first arrivals at 22:06:28. C) Saturated arrivals at higher amplitudes at 22:08:04. d) At 22:12:04 there appears to be no discernable wave arrivals and can see sporadic geyser noise.

Geyser Signal Analysis

Upon analyzing the raw data for time-domain frequency ranges of signals there were some signals that were of particular interest and often occurred in the same southeast portion of the array as illustrated in Figure 5.5. The cluster of stations (003, 021, 022, 040, 041, 042, 061, 062, 063, 085 and 086) showed this behavior for each day approximately every hour. Though the signal is consistently at a range just below 30Hz with some stations fading in signal strength such as Station 085 in Figure 5.5. And in looking at the station placement and consistency of these signals it is definite that these signals are recording some form of anthropogenic noise as they are placed in close proximity around a building.

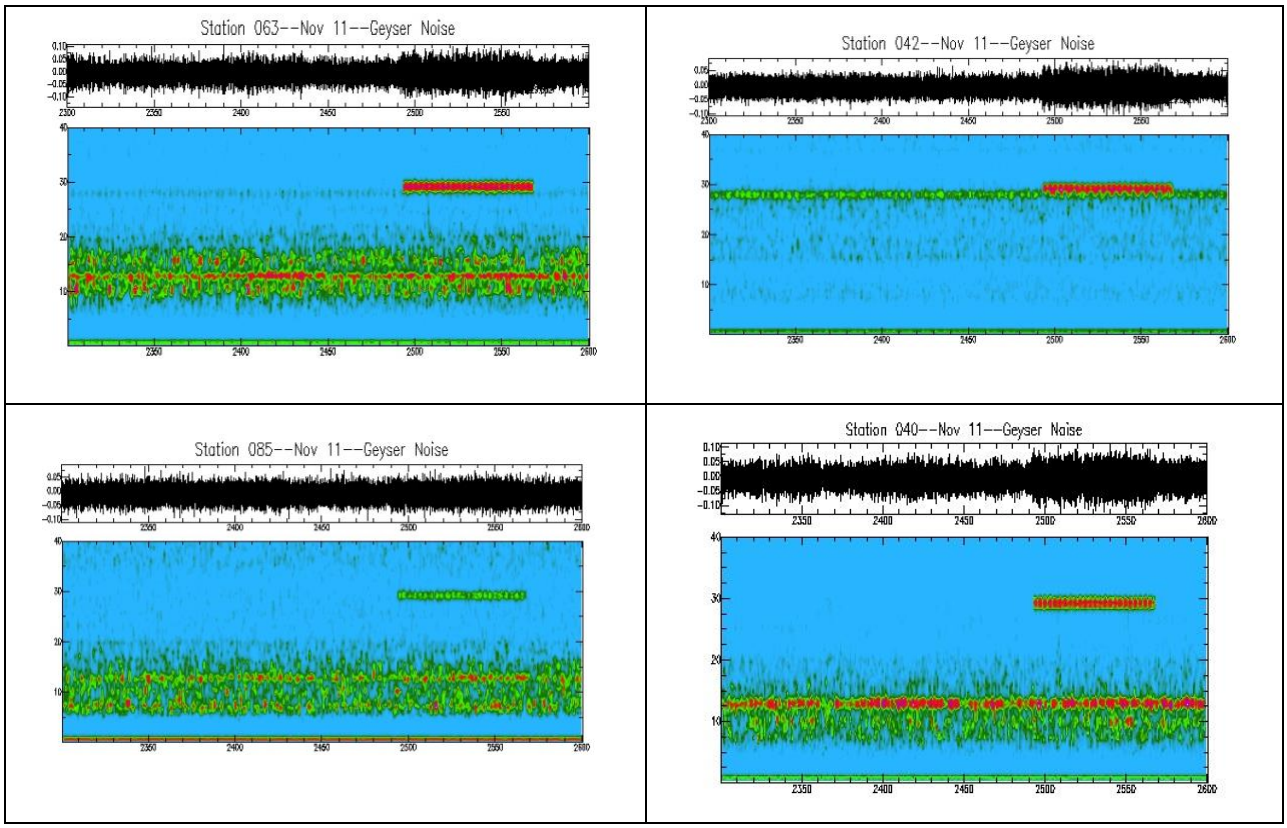

Figure 5.5: Time-Domain Spectrograms of Anomalous Signal

These are spectrograms from stations 040, 042, 063, and 085 that all illustrating a source with cyclical frequency and stays just under 30Hz. The series for all the above examples start at 00:38:20 GMT and end at 00:43:20 GMT.

While combing through this data it becomes apparent there is quite a mixture of natural hydrothermal signal mixed in with anthropogenic signals. The noise associated with buildings and people sometimes stood out more than the constant hum of the hydrothermal features. But one station, number 029, was the one station with cyclical signals that was farthest from structures that could introduce human noise and was placed next to Depression Geyser which is also near Beehive Geyser. Seismograms in Figures 4.5 & 4.6 are an indication of the tireless almost hourly cycles of signal present. Figure 5.7 & 5.8 shows the spectral image of one of these signals from 0.5s to 100Hz and another from 0.5s to 40Hz. In looking at the FFT (figure 5.6) of the signals on several days we see complimenting amplitudes showing the signal continues a steady output.

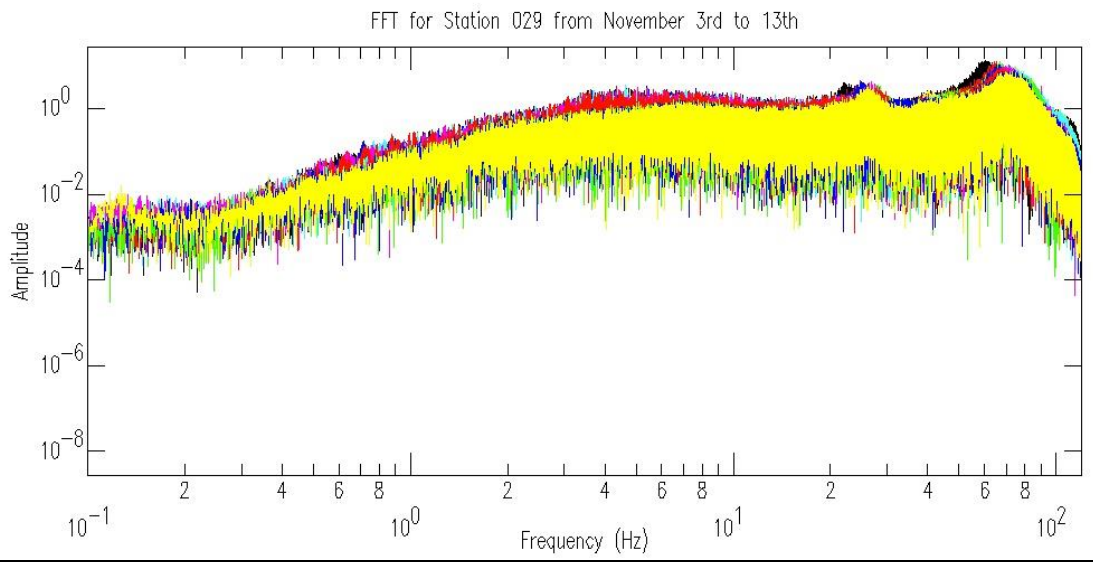

Figure 5.6: Time-Domain Spectrograms of Anomalous Signal
Above is a stacked FFT for station 029 showing geyser signals from November 3rd to 13th. The peak amplitudes retain the same pattern for each day at different time occurences.

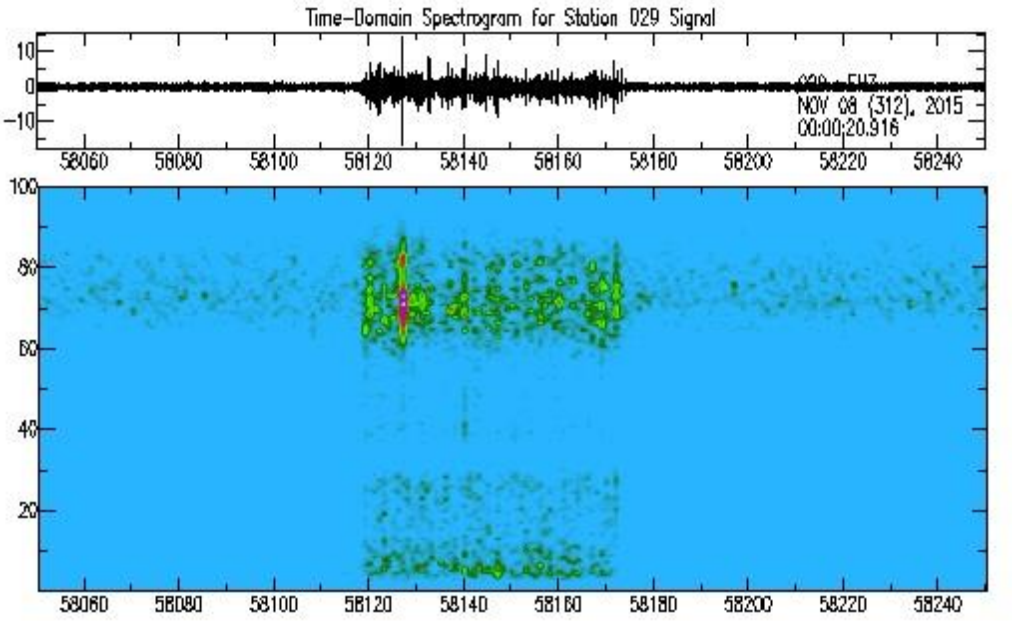

Figure 5.7: Time-Domain Spectrogram of Geyser Signal 100Hz

The November 8th spectrogram y-axis is in Hertz and the x-axis is in seconds which is from 16:07:59 GMT to 16:11:19 GMT with the actual signal having about a one-minute span.

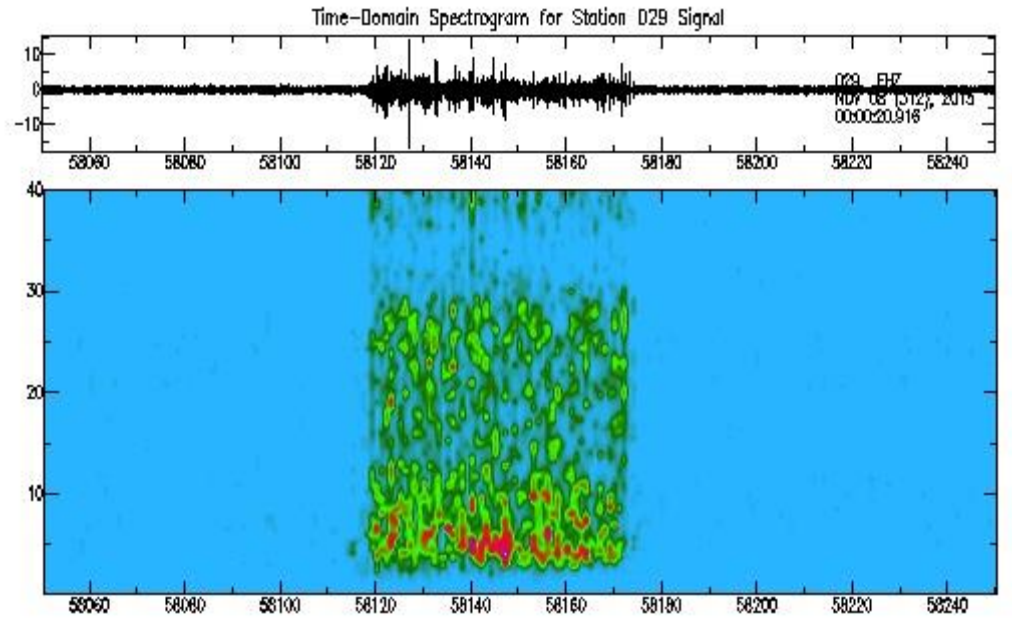

Figure 5.8: Time-Domain Spectrogram of Geyser Signal 40Hz

The November 8th spectrogram y-axis is in Hertz and the x-axis is in seconds which is from 16:07:59 GMT to 16:11:19 GMT with the actual signal having about a one-minute span. This close frequency range of 0.5 to 40Hz gives a better perspective of the strong signal that is under 10Hz.

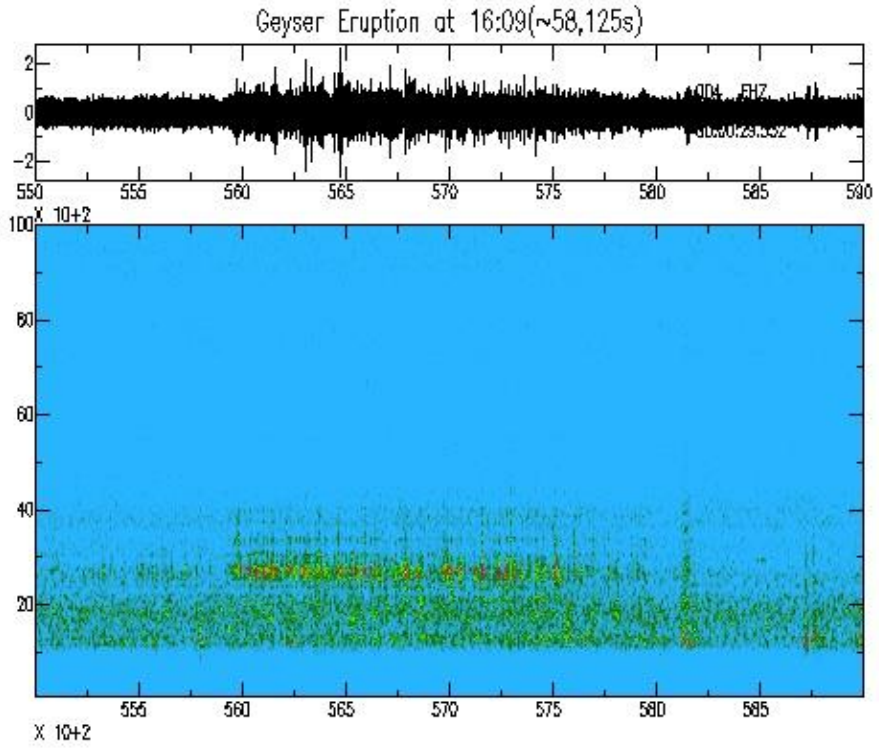

Figure 5.9: Time-Domain Spectrogram of Old Faithful Eruption
This spectrogram from November 5th details the eruption of OFG as seen on station 004. The spectrogram y-axis is in Hertz and the x-axis is in seconds which is from 15:16:40 GMT to 16:23:20 GMT. The longer trail before the actual short geyser eruption is water and steam pressure building up readying for the next eruption. At ~58,125 seconds is the actual eruption.

Old Faithful Geyser eruptions were actually seen on fewer stations especially those farther from the vent. In Figure 5.9, the spectrogram details the stress that occurs right before an actual surface eruption as well as the surface eruption at ~58,125 seconds which is the time of the observed eruption at 16:09UTC. Figure 5.10 shows the seismogram for the same station and same time frame as the spectrogram in figure 5.9 to show the signal seismogram of the build-up and when the eruption occurs. This particular eruption shows an immediate buildup before a geyser eruption approximately 50 minutes before the surface eruption and the spike of the surface eruption lasting a little over 3 minutes.

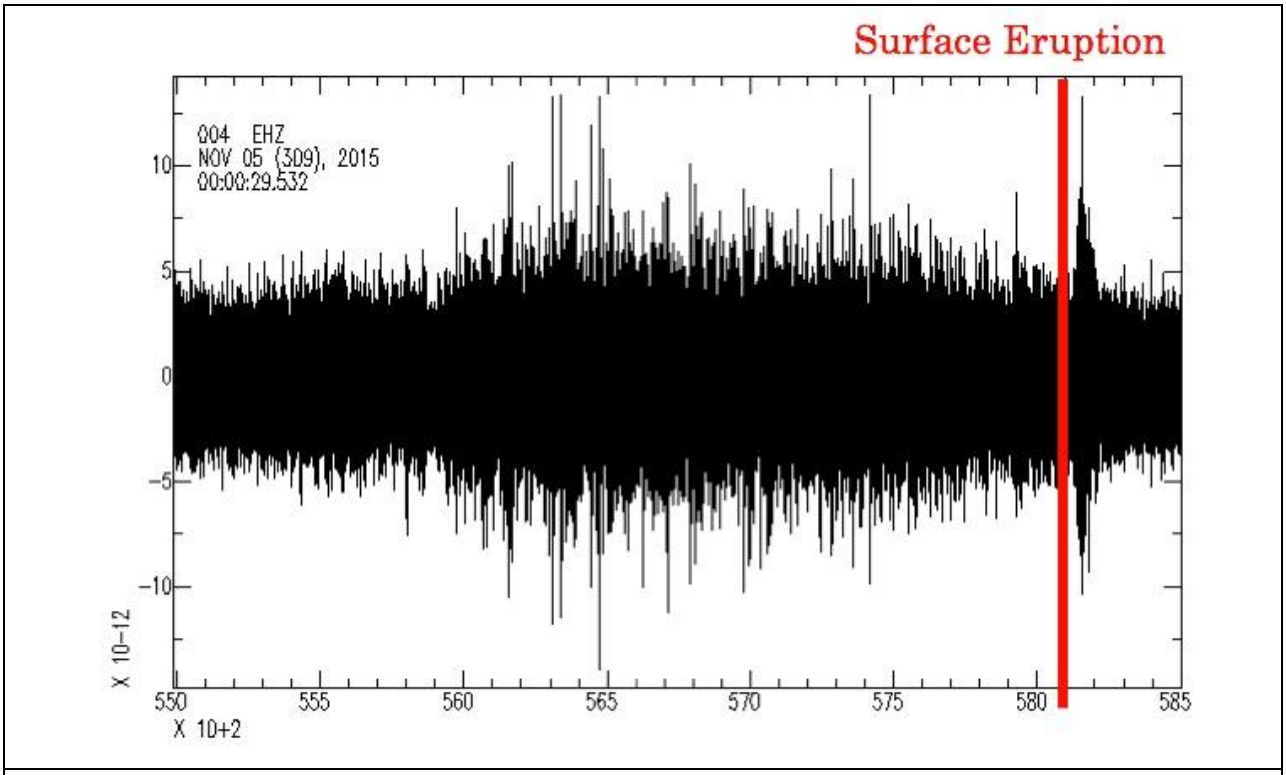

Figure 5.10: Seismogram of Old Faithful Eruption
This seismogram from November 5th details the eruption of OFG as seen on station 004. The y-axis mm/sec and the x-axis is in seconds which is from 15:16:40 GMT to 16:15:00 GMT. The red line indicates the surface eruption which is also noted by the high peak amplitudes. Also, noticeable here is the signal before the actual eruption is roughly a 50 minute occurrence.

One other geyser signal we did look at was the beehive geyser eruption. On November 11th, an eruption was observed at 20:39 UTC. Beehive eruptions are actually quite large but occur much less frequently than OFG eruptions, about 1 or 2 eruptions a day. The seismograms shown in figure 5.11 are an indicator to the shape of the signal for this geyser source. This signal was picked up by quite a few stations concentrated on geyser hill and other parts of the array as seen on the map in figure 5.12. The spectrogram in figure 5.12 demonstrates that the source is concentrated at approximately 70 Hz at station 029.

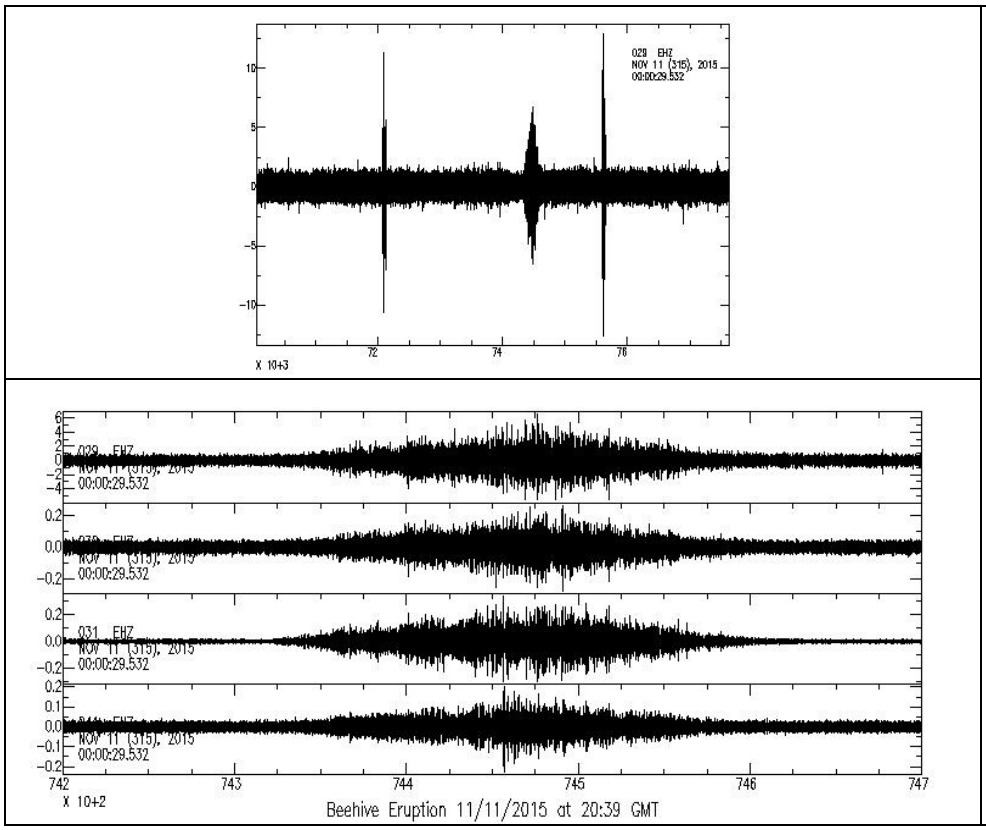

Figure 5.11: Beehive Geyser Eruption Seismograms

The top seismogram was taken from a two-hour window from station 029 showing the beehive geyser signal that occurred at 20:39 UTC between two high amplitude signals from station 029 as discussed previously. The bottom seismograms are a closer view of the beehive signal that starts ~74,325 (20:39:45 UTC) and ends ~74,600 (20:43:20 UTC) with stations (from top to bottom): 029, 030, 031, and 044

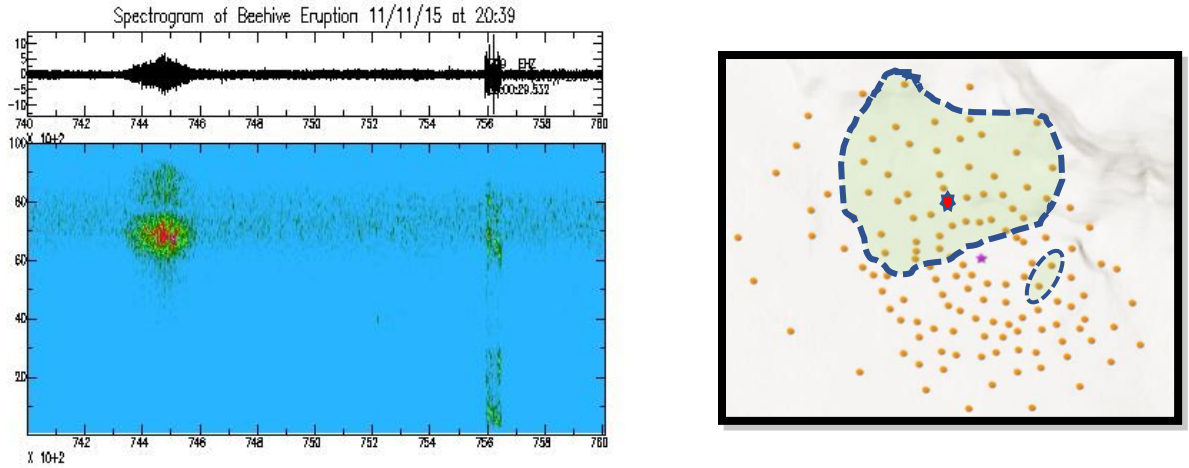

Figure 5.12: Beehive Geyser Spectrogram and Map

On the left is a time-domain spectrogram of the beehive geyser eruption on November 11th as seen on station 029. The energy is concentrated at roughly 70Hz, alongside is the signal source from 029 at ~75,600 seconds. On the right is a map detailing the stations that picked up the beehive eruption (red star), specifically those inside the dashed polygon shapes shaded in light green.

In looking at all the data from the deployment it becomes difficult to discern the noise that is hydrothermal to that which very likely comes from humans. Initially, the analysis of the dataset was to find earthquake sources that were picked up by the local permanent networks. Some of these signals were easy to find on most of the stations but some stations carried too much noise from local sources. As seen on some of these seismograms, microseisms can be seen within the actual earthquake signal especially for those located near noisy geysers or pools. Once it came time to find geyser sources it was a little difficult due to the constant noise from several sources with the exception of station 029 and the sources for eruptions of OFG and beehive. In comparison of the OFG and beehive eruptions it was interesting to see that they differ significantly in their seismic signal shape as seen by the seismograms. Beehive signal was nowhere near as long as the OFG signal which shows tremor signal 50 minutes before the eruption. Beehive had a clean and very apparent signal that tapered at the beginning and end. But more strikingly is that beehive was seen on many more stations than those that are of immediate proximity to OFG. Much of the signals observed in the seismograms were often from human induced sources such as machinery from construction or HVAC systems. And then there are the instances where some nodes did not record data that

With the Aleutian Islands 6.5 MW earthquake it was noted along a line of stations aligned to the southwest wavefront propagation an observation of wave dispersion in stations after passing OFG. It might be possible that the OFG conduit attenuated the waves as they traveled past the conduit system of OFG. Figure 5.13 are detailed 2-minute seismograms of the attenuation incident and can be seen shortly after the first arrivals.

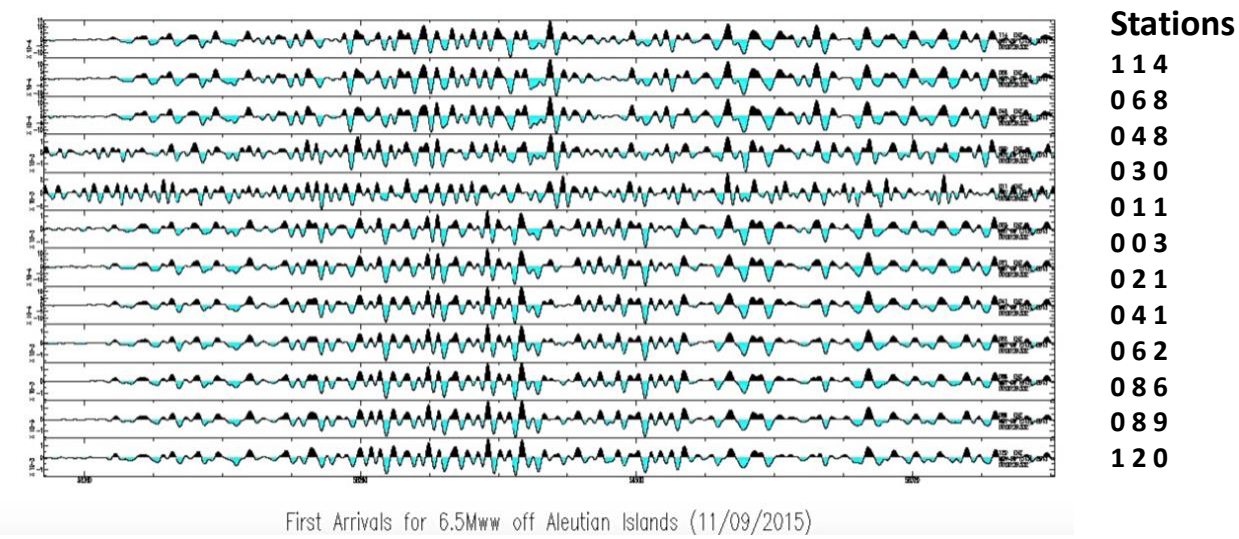

Figure 5.14: Seismograms of Aleutian Islands Earthquake
This seismogram from November 9th show a line of stations aligned to the direction of the earthquake source. From top to bottom stations are: 114, 068, 048, 030, 011, 003, 021, 041, 062, 086, 089, 120. The seismograms are approximately from 16:11:00 UTC to 16:13:00 UTC. Shortly after first arrivals we can see a change in the period of the signals after station 011.

Observations of the GMV movies helped us to understand that sources from very far areas, such as, Chile did not provide detailed information of attenuation since most of the arrivals to the stations are completely vertical and harder to see on an array of 1km aperture. The events that provided some evidence of possible attenuation were the Aleutian Islands 6.5M_W and the local South Wyoming 2.5M_L event. This could be due to the angle at which the waves are arriving to the array are much smaller and thus passing through several of the hydrothermal features and fractures that are at the shallow subsurface of the array.

Chapter 5: Conclusions

Analysis of this dataset as seen through a GMV animation shows changes in velocities as waves arrived to the array was apparent more for close-in earthquakes. The "rotation" of waves as they propagated through the array showed that the southwest quadrant of the array appeared to have slowed velocities in comparison to the velocities in the northeast quadrant of the array that appeared to be faster. And, occurring more often for the GMV's of the Aleutian and South Wyoming earthquakes. This coincides with previous findings of a water reservoir or chamber located southwest of the array. When looking at the large Chile teleseismic events on an array of 1km aperture it is harder to extrapolate information from the GMV's. In looking at geyser signal, the events of Beehive and OFG eruptions provided some insight to the extent of the signal propagation throughout this array. As mentioned before the Beehive geyser eruptions interestingly had farther coverage than the OFG eruptions. The pre-cursor indications of an OFG eruption are almost an hour long before the surface eruption and the proximity of the eruptions are more localized in comparison to the Beehive eruptions. With the analysis of the data we know that there are apparent changes in velocities at the immediate sub-surface.

References

Bryan, T. Scott, and Lee H. Whittlesey. 2008. *The Geysers of Yellowstone.* Fourth. Boulder, CO: University Press of Colorado.

Camp, Victor E., Kenneth L. Pierce, and Lisa A. Morgan. 2015. "Yellowstone plume trigger for Basin and Range extension and coeval emplacement of the Nevada-Columbia Basin magmatic belt." *Geosphere.*

Christiansen, R. L., and H. R., Jr. Blank. 1974. "Geologic Map of the Old Faithful Quadrangle." *Yellowstone National Park, Wyoming: U.S. Geological Survey Geologic Quadrangle.* Vol. 1189. USGS.

Christiansen, R. L., and H. R., Jr. Blank. 1972. "Volcanic stratigraphy of the Quaternary rhyolite plateau in Yellowstone National Park." Professional Paper, United States Geological Survey, 18.

Farrell, J. M., R. Burlacu, P. M. Roberson, J. M. Hale, G. Bobetich, A. Mokhtar, K. D. Koper, R. B. Smith, J. C. Pechmann, and K. L. Pankow. 2015. *Earthquake Activity in the Yellowstone Region October 1 to December 31, 2015.* Quarterly Report, Geology and Geophysics, University of Utah , Salt Lake City: University of Utah.

Farrell, J., R. B. Smith, S. Husen, and T. Diehl. 2014. "Tomography from 26 years of seismicity revealing that the spatial extent of the Yellowstone crustal magma reservoir extends well beyond the Yellowstone caldera." *Geophysical Research Letters* 41: 3068-3073.

Hurwitz, Shaul, Laura E. Clor, R. Blaine McCleskey, D. Kirk Nordstrom, Andrew G. Hunt, and William C. Evans. 2016. "Dissolved gases in hydrothermal (phreatic) and geyser eruptions at Yellowstone National Park, USA." *Geology.*

Hutchinson, Roderick A., James A. Westphal, and Susan W. Keiffer. 1997. "In situ observations of Old Faithful Geyser." *Geology* (Geological Society of America) 25 (10): 875-878.

Kedar, Sharon, and Hiroo Kanamori. 1998. "Bubble collapse as the source of tremor at Old Faithful Geyser." *Journal of Geophysical Research* 103 (B10): 24, 283-284, 299.

Leonard, Tiffany, and Lijun Liu. 2016. "The role of a mantle plume in the formation of Yellowstone volcanism ." *Geophysical Research Letters* 43 (3): 1132-1139.

Lijun, Liu, and Dave R. Stegman. 2011. "Segmentation of the Farallon slab." *Earth and Planetary Science Letters* 311 (1-2): 1-10.

Lijun, Liu, and David R. Stegman. 2012. "Origin of Columbia River flood basalt controlled by propagating rupture of the Farallon slab ." *Nature* 482: 386-389.

Lowenstern, Jacob B., Robert B. Smith, and David P. Hill. 2006. "Monitoring super-volcanoes: geophysical and geochemical signals at Yellowstone and other large caldera systems." *Philisophical Transactions of the Royal Society A* 364: 2055-2072.

Magistrale, Harold, Steven Day, Robert W. Clayton, and Robert Graves. 2000. "The SCEC Southern California Reference Three-Dimensional Seismic Velocity Model Version 2." *Bulletin fo the Seismological Society of America* 90 (6B): S65-S76.

Mastin, Larry G., Alexa R. Van Eaton, and Jacob B. Lowenstern. 2014. "Modeling ash fall distribution from a Yellowstone supereruption." *Geochemistry, Geophysics, Geosystems* (American Geophysical Union) 15 (8): 3459-3475.

My Yellowstone Park Staff Writer. 2017. *My Yellowstone Park.* National Park Trips Media. Accessed August 2017. https://www.yellowstonepark.com/things-to-do/see-old-faithful-and-most-the-worlds-geysers-in-yellowstone-national-park-upper-geyser-basin.

National Geographic. 2017. *Inside Yellowstone's Supervolcano.* Edited by Duncan Foley, Robert Fournier, Henry Heasler, Cheryl Jaworowski, Jacob Lowenstern, Robert B. Smith and Jamie Farrell. Manuel Canales, Daisy Chung, Daniela Santamarina and Swordsweeper Industries. June. Accessed June 2017. https://www.nationalgeographic.com/magazine/2016/05/yellowstone-national-parks-supervolcano-animation/.

National Park Service. 2017. *Frequently Asked Questions: Old Faithful Geyser.* U.S. Department of Interior. January. https://www.nps.gov/yell/learn/nature/oldfaithfulgeyserfaq.htm.

—. n.d. *Yellowstone Geology.* U.S. Depatment of Interior. Accessed March 2016. https://www.nps.gov/yell/learn/nature/volcano.html.

—. 2017. *Yellowstone Volcano.* April 24. Accessed September 12, 2017. https://www.nps.gov/yell/learn/nature/volcano.htm.

Old Faithful Science Review Panel. 2014. *Hydrogeology of the Old Faithful Area, Yellowstone National Park, Wyoming, and it Relevance to Natural Resources and Infrastructure.* Open-File Report, U.S. Geological Survey, 28.

Parsons, K. L., G. A. Thompson, and R. P. Smith. 1994. "Mantle Plume influence on the Neogene uplift and extension of the U.S. western Cordillera." *Geology* 22: 83-86.

Peng, Xiaohua, and Eugene D. Humphreys. 1998. "Crustal velocity structure across the eastern Snake River Plain and the Yellowstone Swell." *Journal of Geophysical Research* 103 (B4): 7171-7186.

Pierce, K. L., and L. A. Morgan. 1992. "The track of the Yellowstone hotspot: Volcanism, faulting, and uplift." Edited by P. K. Link, M. A. Kuntz and L. B. Platt. *Regional Geology of Eastern Idaho and Western Wyoming: Geological Society of America Memoir* 179: 1-53.

Robinson, Enders A., Tariq S. Durrani, and Lloyd G. Peardon. 1986. *Geophysical Signal Processing.* Englewood Cliffs, NJ: Prentice-Hall.

Smith, R. B., and L. Siegel. 2000. *Windows into the Earth's Interior: The geological story of Yellowstone and Grand Teton National Parks.* Oxford: Oxford University Press.

Smith, R., M. Jordan, B. Steinberger, C. Puskas, J. Farrell, G. Waite, S. Husen, W. Chang, and R. O'Connell. 2009. "Geodynamics of the Yellowstone hotspot and mantle plume: Seismic and GPS imaging, kinematics, and mantle flow." Edited by Science & Technology Collection. *Journal of Volcanology & Geothermal Research* (EBSCOhost) 188 (1-3): 26-56.

Trabant, C., A. R. Hutko, M. Bahavar, R. Karstens, T. Ahern, and R. Aster. 2012. "Data Products at the IRIS DMC: Stepping Stones for Research and Other Applications." *Seismological Research Letters* (83(5)): 846-854.

U.S. Geological Survey. 2016. *USGS: Volcano Hazards Program.* June 2. Accessed February 2017. https://volcanoes.usgs.gov/volcanoes/yellowstone/.

Vandemeulebrouck, J., P. Roux, and E. Cross. 2013. "The plumbing of Old Faithful Geyser revealed by hydrothermal tremor." *Geophysical Research Letters* 40: 1989-1993.

Wood, Charles A., and Jurgen Kienle. 1990. *Volcanoes of North America: United States and Canada.* Cambridge: Cambridge University Press.

Wu, S.-M., K. M. Ward, F. C. Lin, J. Farrell, M. Karplus, and R. B. Smith. 2017. "Anatomy of Old Faithful from subsurface seismic imaging of the Yellowstone Upper Geyser Basin." *Geophysical Research Letters* 44.

Yellowstone National Park (NPS). 2014. *Old Faithful Area Tour-Beehive Geyser.* U.S. Department of Interior. Accessed August 13, 2017. https://www.nps.gov/features/yell/tours/oldfaithful/beehive_work.htm.

Appendix

Python Script for Process Automation

One example of earthquake data process automation with Python script: (Script and other SAC resources are available online with the IRIS website: http://ds.iris.edu/files/sac-manual/manual.html)

eq65GMV_KZtime.py

```
#!/usr/bin/env python
# script to prep SAC files for GMV

import subprocess
import glob

p = subprocess.Popen(['sac'],
                     stdout = subprocess.PIPE,
                     stdin  = subprocess.PIPE,
                     stderr = subprocess.STDOUT )


s = "echo on\n"
for filename in glob.glob("/Users/user/Desktop/1109SAC/decimated4/*.sac"):
    s += '''
        cut 58230 58450
        read %(file)s
        qdp off
        rmean
        bp bu p 2 n 4 c 0.09 0.9
        taper
        ch nzhour 16
        ch nzmin 10
        ch nzsec 30
        ch nzmsec .000
        write %(file)s.eq65
    ''' % ( {'file': filename } )
s += "quit\n"
out = p.communicate( s )
print out[0]

```

*Note-There are errors associated with writing new header information such as KZTIME, which applies to the nzhour, nzmin, nzsec, and nzmsec. A shift in time will occur and could affect the type of processing results that you are seeking.

SAC Sample Commands

In prepping your data: One very important detail is removing the instrument response from your dataset. This will create a much more coherent signal to work with. The poles and zeros file contains a file with similar information as stated below. You must use the appropriate channel for each corresponding channel, this one here is for the vertical (Z) channel. In some cases, the file will be the same for all three channels. When downloading data from Wilber you may select to receive the SACPZ file. In the sac sample below, you must be cognizant of the corner frequencies you are selecting as to avoid alienating the signal frequency range you are looking for, and also, to avoid cutting beyond the frequency range of the instrument.

```
* **********************************
* NETWORK   (KNETWK): YW
* STATION    (KSTNM): 1002
* LOCATION   (KHOLE):
* CHANNEL   (KCMPNM): DPZ
* CREATED           : 2017-11-16T17:41:42
* START             : 2016-06-21T00:00:00
* END               : 2016-07-27T23:59:59
* DESCRIPTION       : Node at Wavefields Community Experiment, OK, USA
* LATITUDE          : 36.622301
* LONGITUDE         : -97.739831
* ELEVATION         : 322.2
* DEPTH             : 0.0
* DIP               : 180.0
* AZIMUTH           : 0.0
* SAMPLE RATE       : 250.0
* INPUT UNIT        : M
* OUTPUT UNIT       : COUNTS
* INSTTYPE          : Zland 3C geophone/Zland 3C DAS est w/o anti-alias
* INSTGAIN          : 7.671440e+01 (M/S)
* COMMENT           : 1002 1002
* SENSITIVITY       : 1.029640e+09 (M/S)
* A0                : 9.998130e-01
* **********************************
ZEROS   3
        +0.000000e+00  +0.000000e+00
        +0.000000e+00  +0.000000e+00
        +0.000000e+00  +0.000000e+00
POLES   2
        -2.199000e+01  +2.243000e+01
        -2.199000e+01  -2.243000e+01
CONSTANT       1.029447e+09
```

```
SAC> r *.sac
001.EHZ.11092015.sac 002.EHZ.11092015.sac 003.EHZ.11092015.sac 004.EHZ.11092015.sac 005.EHZ.11092015.sac
006.EHZ.11092015.sac 007.EHZ.11092015.sac 008.EHZ.11092015.sac 009.EHZ.11092015.sac 010.EHZ.11092015.sac
011.EHZ.11092015.sac 012.EHZ.11092015.sac 013.EHZ.11092015.sac 014.EHZ.11092015.sac 015.EHZ.11092015.sac
016.EHZ.11092015.sac 017.EHZ.11092015.sac 018.EHZ.11092015.sac 019.EHZ.11092015.sac 020.EHZ.11092015.sac
021.EHZ.11092015.sac 022.EHZ.11092015.sac 023.EHZ.11092015.sac 024.EHZ.11092015.sac 025.EHZ.11092015.sac
026.EHZ.11092015.sac 027.EHZ.11092015.sac 028.EHZ.11092015.sac 029.EHZ.11092015.sac 030.EHZ.11092015.sac
031.EHZ.11092015.sac 032.EHZ.11092015.sac 033.EHZ.11092015.sac 034.EHZ.11092015.sac 035.EHZ.11092015.sac
036.EHZ.11092015.sac 037.EHZ.11092015.sac 038.EHZ.11092015.sac 039.EHZ.11092015.sac 040.EHZ.11092015.sac
041.EHZ.11092015.sac 042.EHZ.11092015.sac 043.EHZ.11092015.sac 044.EHZ.11092015.sac 045.EHZ.11092015.sac
046.EHZ.11092015.sac 047.EHZ.11092015.sac
048.EHZ.11092015.sac 049.EHZ.11092015.sac 050.EHZ.11092015.sac 051.EHZ.11092015.sac 052.EHZ.11092015.sac
053.EHZ.11092015.sac 054.EHZ.11092015.sac 055.EHZ.11092015.sac 056.EHZ.11092015.sac 057.EHZ.11092015.sac
058.EHZ.11092015.sac 059.EHZ.11092015.sac 060.EHZ.11092015.sac 061.EHZ.11092015.sac 062.EHZ.11092015.sac
063.EHZ.11092015.sac 065.EHZ.11092015.sac 066.EHZ.11092015.sac 067.EHZ.11092015.sac 068.EHZ.11092015.sac
069.EHZ.11092015.sac 070.EHZ.11092015.sac 071.EHZ.11092015.sac 072.EHZ.11092015.sac 073.EHZ.11092015.sac
074.EHZ.11092015.sac 075.EHZ.11092015.sac 076.EHZ.11092015.sac 077.EHZ.11092015.sac 078.EHZ.11092015.sac
079.EHZ.11092015.sac 080.EHZ.11092015.sac 081.EHZ.11092015.sac 082.EHZ.11092015.sac 083.EHZ.11092015.sac
084.EHZ.11092015.sac 085.EHZ.11092015.sac 086.EHZ.11092015.sac 089.EHZ.11092015.sac 090.EHZ.11092015.sac
091.EHZ.11092015.sac 092.EHZ.11092015.sac 093.EHZ.11092015.sac 094.EHZ.11092015.sac 095.EHZ.11092015.sac
096.EHZ.11092015.sac 097.EHZ.11092015.sac
098.EHZ.11092015.sac 099.EHZ.11092015.sac 100.EHZ.11092015.sac 101.EHZ.11092015.sac 102.EHZ.11092015.sac
103.EHZ.11092015.sac 104.EHZ.11092015.sac 105.EHZ.11092015.sac 106.EHZ.11092015.sac 107.EHZ.11092015.sac
108.EHZ.11092015.sac 109.EHZ.11092015.sac 111.EHZ.11092015.sac 112.EHZ.11092015.sac 113.EHZ.11092015.sac
114.EHZ.11092015.sac 115.EHZ.11092015.sac 116.EHE.11092015.sac 116.EHN.11092015.sac 116.EHZ.11092015.sac
117.EHZ.11092015.sac 118.EHZ.11092015.sac 119.EHZ.11092015.sac 120.EHZ.11092015.sac 121.EHZ.11092015.sac
122.EHZ.11092015.sac 123.EHZ.11092015.sac 124.EHZ.11092015.sac 125.EHZ.11092015.sac 126.EHZ.11092015.sac
127.EHZ.11092015.sac 128.EHZ.11092015.sac 129.EHZ.11092015.sac 130.EHZ.11092015.sac 131.EHZ.11092015.sac
132.EHZ.11092015.sac 133.EHZ.11092015.sac 134.EHZ.11092015.sac 135.EHZ.11092015.sac 144.EHZ.11092015.sac
148.EHZ.11092015.sac
SAC> rmean
SAC> taper w 0.01
SAC> transfer from polezero S NODE_SAC_PZ freq 0.01 0.015 50 60
 ERROR  108: File does not exist: NODE_SAC_PZ
SAC> transfer from polezero S NODE_SAC_PZ.txt freq 0.01 0.015 50 60
```

Volcanic Explosivity Index

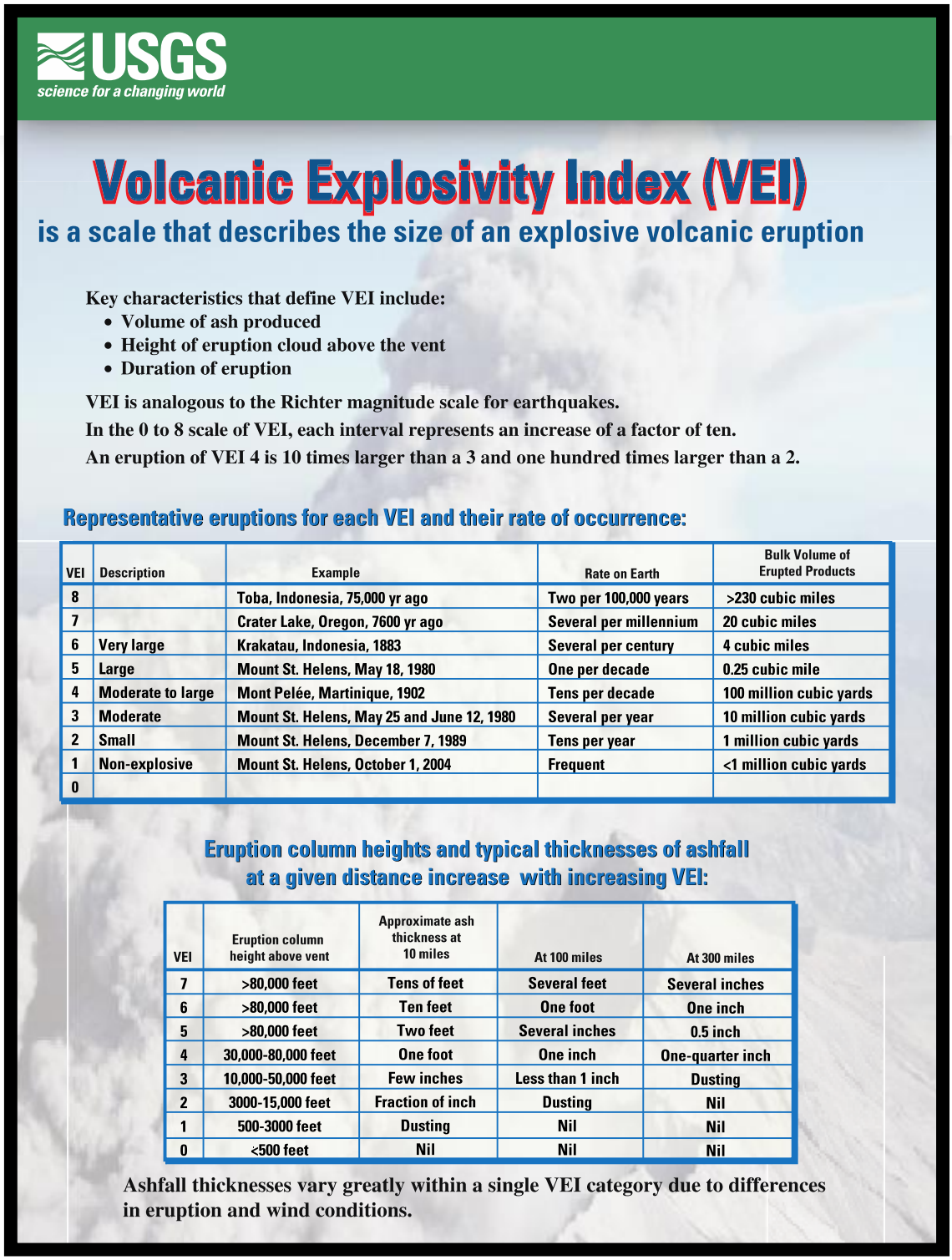

USGS
science for a changing world

Volcanic Explosivity Index (VEI)

is a scale that describes the size of an explosive volcanic eruption

Key characteristics that define VEI include:

- Volume of ash produced
- Height of eruption cloud above the vent
- Duration of eruption

VEI is analogous to the Richter magnitude scale for earthquakes.
In the 0 to 8 scale of VEI, each interval represents an increase of a factor of ten.
An eruption of VEI 4 is 10 times larger than a 3 and one hundred times larger than a 2.

Representative eruptions for each VEI and their rate of occurrence:

VEI	Description	Example	Rate on Earth	Bulk Volume of Erupted Products
8		Toba, Indonesia, 75,000 yr ago	Two per 100,000 years	>230 cubic miles
7		Crater Lake, Oregon, 7600 yr ago	Several per millennium	20 cubic miles
6	Very large	Krakatau, Indonesia, 1883	Several per century	4 cubic miles
5	Large	Mount St. Helens, May 18, 1980	One per decade	0.25 cubic mile
4	Moderate to large	Mont Pelée, Martinique, 1902	Tens per decade	100 million cubic yards
3	Moderate	Mount St. Helens, May 25 and June 12, 1980	Several per year	10 million cubic yards
2	Small	Mount St. Helens, December 7, 1989	Tens per year	1 million cubic yards
1	Non-explosive	Mount St. Helens, October 1, 2004	Frequent	<1 million cubic yards
0				

Eruption column heights and typical thicknesses of ashfall at a given distance increase with increasing VEI:

VEI	Eruption column height above vent	Approximate ash thickness at 10 miles	At 100 miles	At 300 miles
7	>80,000 feet	Tens of feet	Several feet	Several inches
6	>80,000 feet	Ten feet	One foot	One inch
5	>80,000 feet	Two feet	Several inches	0.5 inch
4	30,000-80,000 feet	One foot	One inch	One-quarter inch
3	10,000-50,000 feet	Few inches	Less than 1 inch	Dusting
2	3000-15,000 feet	Fraction of inch	Dusting	Nil
1	500-3000 feet	Dusting	Nil	Nil
0	<500 feet	Nil	Nil	Nil

Ashfall thicknesses vary greatly within a single VEI category due to differences in eruption and wind conditions.

Numbered Station Map of the Array

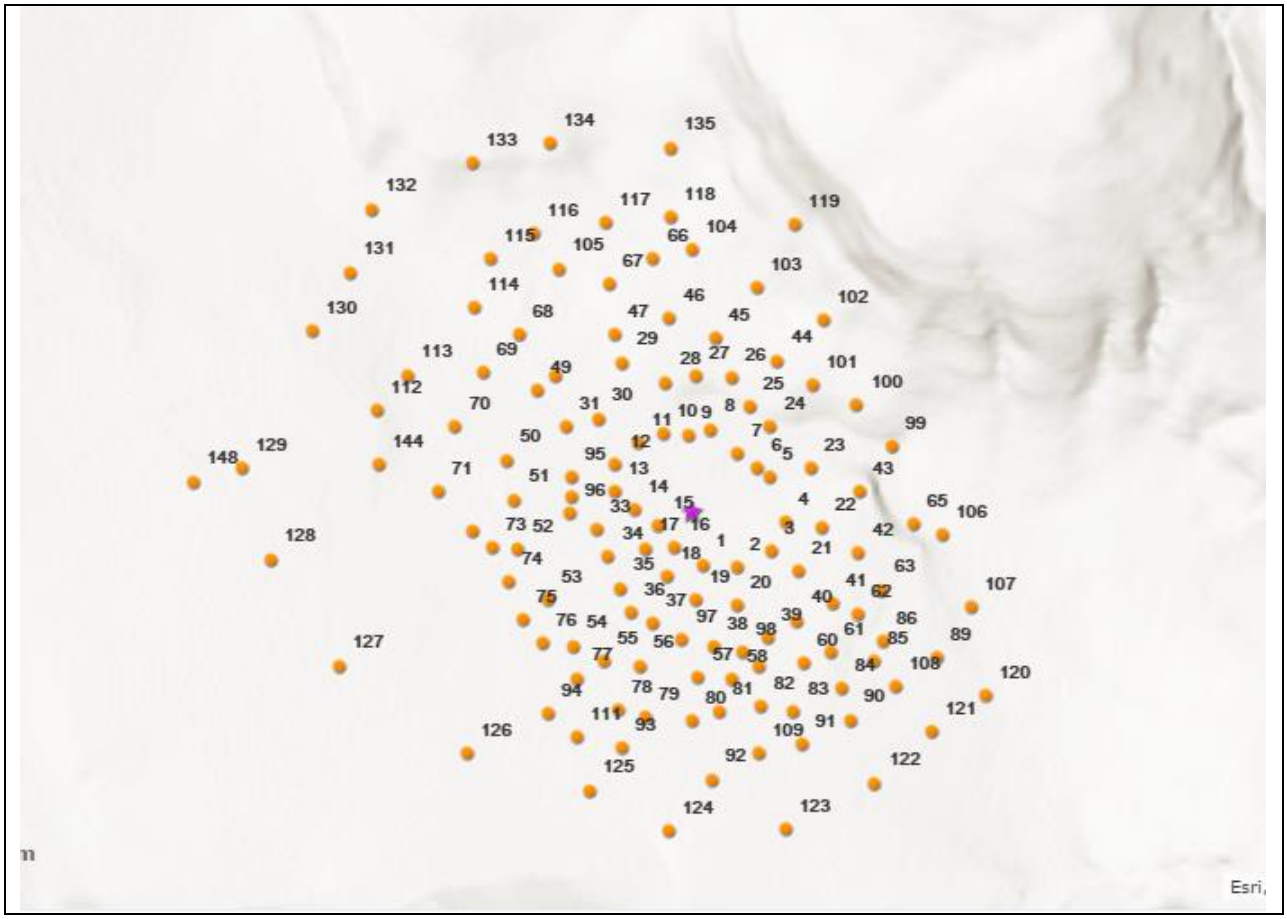

Curriculum Vitae

Ms. Susana Garcia earned her Bachelor's degree in Geology from California State Polytechnic University at Pomona in 2012 where she followed a Geophysics track. A native of El Paso, TX, she moved back in 2012 and later decided to return to school to obtain her Master's in Geophysics at UTEP's outstanding program and completing in 2017. During her time at UTEP she was able to participate in a large seismic deployment at Yellowstone National Park and partake in some educational outreach activities within the department. She received an Air Quality summer internship in 2016 with the U.S. Environmental Protection Agency allowing her to use her acquired skills in an interdisciplinary manner.

Permanent address: susana.i.garcia13@gmail.com

This thesis was typed by the author.